Geological Magazine

www.cambridge.org/geo

Original Article

Cite this article: Maravelis AG, Offler R, Botziolis C, Pantopoulos G, Scott A, Landenberger B, and Collins WJ (2023) Provenance of a Late Permian retroarc foreland basin along the eastern Gondwanan margin: northern Sydney Basin, eastern Australia. *Geological Magazine* **160**: 1535–1555. https://doi.org/10.1017/S0016756823000535

Received: 2 June 2023
Revised: 5 August 2023
Accepted: 21 August 2023
First published online: 26 September 2023

Keywords:
provenance; tectonic setting; retroarc foreland basin; Permian; Northern Sydney Basin

Corresponding author:
Angelos G. Maravelis;
Email: angmar@geo.auth.gr

Provenance of a Late Permian retroarc foreland basin along the eastern Gondwanan margin: northern Sydney Basin, eastern Australia

Angelos G. Maravelis[1], Robin Offler[2], Chrysanthos Botziolis[3], George Pantopoulos[4], Alexandra Scott[2], Bill Landenberger[2] and William J. Collins[5]

[1]Department of Geology, Aristotle University of Thessaloniki, Thessaloniki, Greece; [2]School of Environmental and Life Sciences, University of Newcastle, Callaghan NSW, Australia; [3]Laboratory of Sedimentology, Department of Geology, University of Patras, Rion, Greece; [4]Department of Earth Sciences “Ardito Desio”, University of Milan, Milan, Italy and [5]The Institute for Geoscience Research (TIGeR), Department of Applied Geology, Curtin University, Perth WA, Australia

Abstract

The Upper Permian sedimentary successions in the northern Sydney Basin have been the subject of several stratigraphic, sedimentological and coal petrographic studies, and recently, extensive U-Pb zircon dating has been carried out on tuffs in the Newcastle Coal Measures. However, detailed petrographic and geochemical studies of these successions are lacking. These are important because a major change in tectonic setting occurred prior to the Late Permian because of the Hunter-Bowen Orogeny that caused the uplift of the Carboniferous and Devonian successions in the Tamworth Group and Tablelands Complex adjacent to the Sydney Basin. This should be reflected in the detrital makeup of the Upper Permian rocks. This study provides data that confirms major changes did take place at this time. Petrographic analysis indicates that the source area is composed of sedimentary, felsic volcanic and plutonic and low-grade metamorphic rocks. Conglomerate clast composition analysis confirms these results, revealing a source region that is composed of felsic volcanics, cherts, mudstones and sandstones. Geochemical analysis suggests that the sediments are geochemically mature and have undergone a moderate degree of weathering. The provenance data presented in this paper indicate that the southern New England Orogen is the principal source of detritus in the basin. Discrimination diagrams confirm that the source rocks derive from an arc-related, contractional setting and agree with the provenance analyses that indicate sediment deposition in a retroarc foreland basin. This study offers new insights on the provenance and tectonic setting of the Northern Sydney Basin, eastern Australia.

1. Introduction

The sedimentary record in retroarc foreland regions provides information about convergence margins and associated characteristics, such as the advance and/or retreat of the accretionary prisms and the formation of magmatic arcs. The documentation of the interaction between subducting lithospheric plates and the formation and evolution of sedimentary basins on the overriding plates was a major advance in understanding plate tectonics (Dickinson, 1995; Busby *et al.* 1998). Retroarc foreland basins record information about the relative movements between the trench, the subducting and the overriding plate and their study led to the development of evolutionary models (e.g. Horton, 2022).

By any means, unravelling the type and origin of sedimentary basins is not straightforward and requires the integration of various lines of evidence. The implementation of data from sedimentary petrography and geochemistry are routinely employed in basin analysis studies (Armstrong-Altrin, 2009; Maravelis *et al.* 2015; Adekola, *et al.* 2018; Khazaei *et al.* 2018). Processes such as sorting, weathering and diagenesis affect the geochemical signatures of clastic sedimentary rocks (Weltje, 2006). Thus, immobile elements (e.g. REE, Zr, Y, Th and Ti), which are least affected by weathering are considered as the most credible provenance indicators (McLennan, 1989; Hessler & Lowe, 2006). In addition to geochemistry, conglomerates contain large clasts of the source rocks and have been proven very useful in provenance analysis (Bradshaw *et al.* 2012). Even though provenance data are very important in sedimentary basin analysis, robust geotectonic interpretation requires integration of additional field evidence including sedimentological, sequence stratigraphic and palaeocurrent data (Maravelis *et al.* 2016). Investigations have also questioned the ability of geochemical discrimination diagrams to provide unequivocal interpretations about the tectonic setting of a study region (Ryan & Williams, 2007; Armstrong-Altrin, 2009; Zaid & Gahtani, 2015). These discussions strengthen

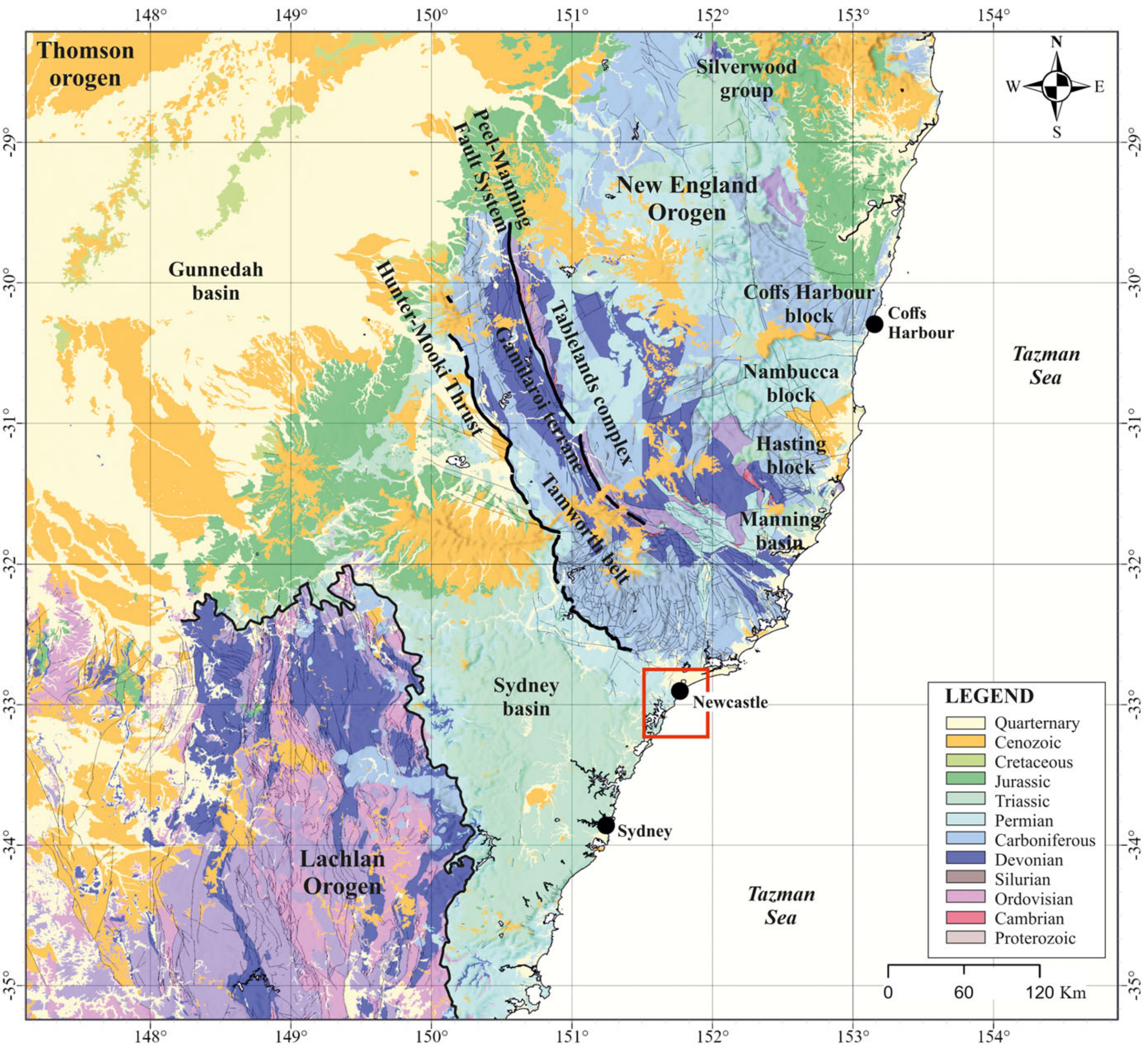

Figure 1. (Colour online) Geological map of NEO and surrounding regions depicting the distribution of the Tablelands Complex and the Tamworth Belt (accretionary prism and forearc basin respectively, Leitch, 1974; Korsch, 1977).

the notion that the geochemical interpretations must be compatible with the actual sedimentary record (Maravelis *et al.* 2015, 2016).

The Sydney Basin (SB) is a suitable case study to evaluate the impact of subduction-associated processes in the evolution of sedimentary basins. The SB is the southern margin of the larger Bowen-Gunnedah-Sydney Basin (Glen, 2005) and is positioned between the New England Orogen (NEO) to the northeast and the Lachlan Orogen to the southwest (Fig. 1, Roberts & Engel, 1987). This study is conducted in the northern part of the SB on the Upper Permian sedimentary rocks that belong to the Newcastle Coal Measures (NCM, Fig. 2). The NCM are divided into three sub-groups (Boolaroo, Adamstown and Lambton Sub-groups), but recent sedimentological, sequence stratigraphic and geochronological studies indicate stratigraphic repetition (Breckenridge *et al.* 2019; Maravelis *et al.* 2020; Melehan *et al.* 2021). It has been proposed that the three sub-groups that make up the NCM could be merged into the Lambton Sub-group that is representative of the NCM (Maravelis *et al.* 2020, Fig. 2). The contribution of NEO and Lachlan Orogens to the sedimentation of the NCM has not been geochemically determined because studies to establish the provenance are lacking.

In the light of the absence of such data, this research provides petrographic and geochemical data, along with data from conglomerate clast composition analysis to define the provenance and tectonic setting of the Upper Permian succession in the NCM. The results reveal that particular units within the NEO contributed to the composition of the succession, indicating a felsic to intermediate source rock that provided detritus in a retroarc foreland basin. The outcomes are then integrated with published palaeocurrent and sequence stratigraphic data to offer a framework for understanding the geodynamic processes that controlled the evolution of eastern Gondwana during the Late Permian.

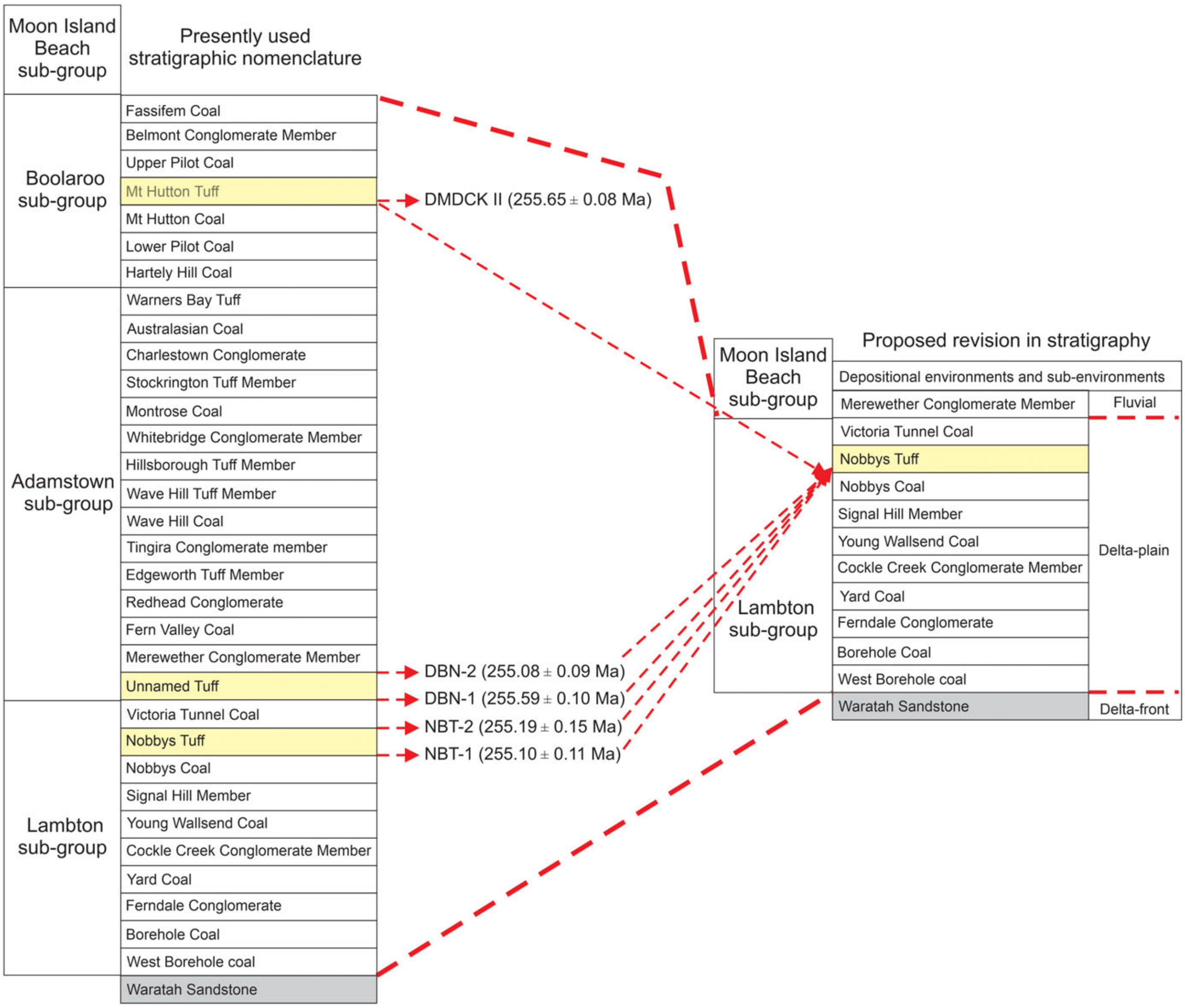

Figure 2. (Colour online) Comparable diagrams illustrating the differences between the current and revised stratigraphic framework in the NSB (from Maravelis *et al.* 2020). The revised stratigraphic model condenses the NCM stratigraphy, suggesting the existence of the Lambton Sub-group that is represented by the deltaic setting and the Moon Island Beach Sub-group that includes (at least at its basal part) the fluvial portion of the succession.

2. Geological setting

During the Permian to early Triassic time, Australia was part of eastern Gondwana, the southern hemisphere component of supercontinent Pangea, located in high southern palaeolatitudes (Veevers, 2013). The SB is ~1600 km long (Glen, 2005), and stratigraphic equivalents can be traced through Antarctica, South Africa and South America as the foreland basin to the Gondwanide Orogen (Veevers, 2013). The SB is underlain by two different basement types and displays an asymmetric geometry with the thickest succession occurring in the northeast. In the southwest, the SB overlies the Early-Middle Palaeozoic Lachlan Orogen, and to the northeast, the Late Palaeozoic NEO underlies the SB (Jessop *et al.* 2019).

The SB initiated as a continental backarc in the Late Carboniferous-Early Permian (Shaanan & Rosenbaum, 2018), confirmed by the trace element chemistry of gabbroic and basaltic rocks (Jenkins *et al.* 2002; McKibbon *et al.* 2016). During the later stages of the Early Permian, a mixture of post-rift subsidence and the cessation of loading caused a westward marine transgression over the Lachlan Orogen to the southwest during subduction of an east-facing convergent margin in the southern NEO to the northeast (Fielding *et al.* 2001). Subsequently, the NCM experienced subsequent conversion to a foreland basin by progressive west-directed thrusting and folding (Li *et al.* 2012; Li & Rosenbaum, 2014; Philips *et al.* 2015), as evidenced by the geometry and kinematics of the Late Permian folds and faults in the southern NEO and SB (Collins, 1991; Landenberger *et al.* 1995; Jenkins & Offler, 1996). The Late Permian deformational pattern in the southern NEO is interpreted as the result of a single but complex compressive tectonic event, the Hunter-Bowen Orogeny, 265–250 Ma ago (Jenkins *et al.* 2002; Hoy & Rosenbaum, 2017).

The uplifted and over-thrusted NEO became a major sediment contributor to the SB during the deposition of sediments in the NCM, and its evolution was responsible for the evolution of the NCM as a foreland basin (Korsch & Totterdell, 2009). During the evolution of the SB into a foreland basin, sediments display

https://doi.org/10.1017/S0016756823000535 Published online by Cambridge University Press

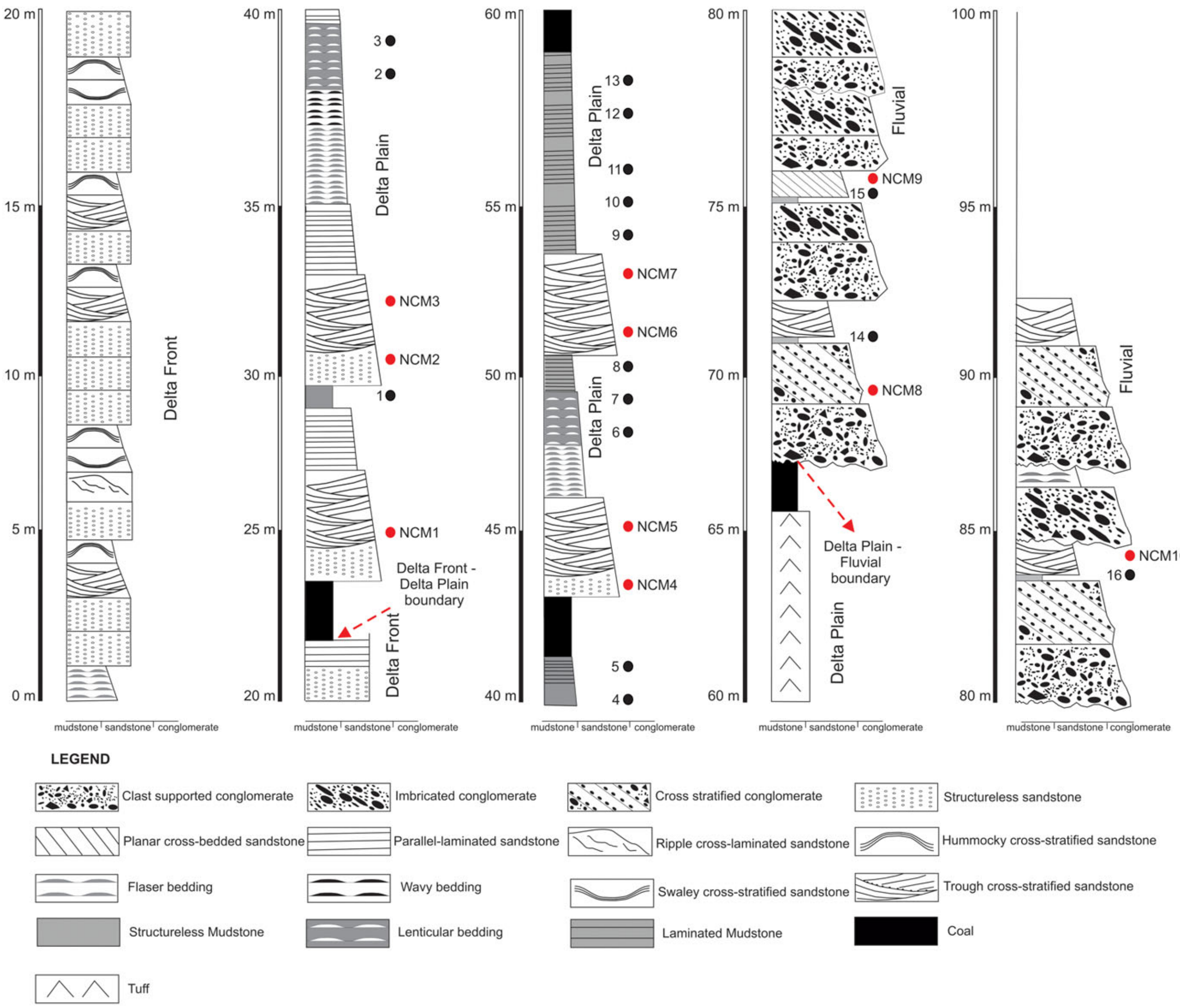

Figure 3. (Colour online) Stratigraphic column that portrays the temporal development of the studied sedimentary succession. Note the decrease in water depth as documented by the shift from delta-front to delta-plain sediments and finally to fluvial deposits (from Breckenridge *et al.* 2019).

rapid lateral and vertical facies changes, which result from eustatically and tectonically controlled regressions and transgressions (Herbert & Helby, 1980). During the Middle to Late Triassic, fold and thrust belts dissected the SB, in response to westward migrating thrust fronts with associated crustal shortening (Babaahmadi *et al.* 2017). This deformation terminated the deposition in the SB during the Middle-Triassic time (Herbert & Helby, 1980). In this setting, the evolution of the SB is remarkably similar to the evolution of other contemporary sedimentary basins in southern Gondwana, including the Karoo Basin in southern Africa (Catuneanu, 2004) and the foreland systems of South America (Menegazzo *et al.* 2016). Similar net progradation of the shoreline has also been documented in the Karoo Basin, although with less evidence for tidal activity (Rubidge *et al.* 2000).

3. Materials and methods

In terms of the involved depositional environments and subenvironments, the NCM consist of delta-front deposits that evolve upwards into delta-plain facies and finally into fluvial deposits, documenting a regional shallowing-upward trend (Fig. 3). This study deals with the delta-plain and fluvial portions of the sedimentary succession. Petrographic analyses were performed on ten (10) fine- to medium-grained sandstone samples that were collected from outcrops (sample NCM1 to NCM 10), whereas conglomerate clast composition analysis was performed at seven (7) outcrops (Figs. 3 and 4). Further, sixteen (16) samples were collected for geochemical analysis (Figs. 3 and 4).

Petrographic analysis was conducted using the Gazzi-Dickinson point-counting method (Dickinson & Suczek, 1979; Ingersoll *et al.* 1984), on a B-1000 Series Optika Italy polarizing microscope. At least 300 grains per section were examined, and features such as grain shape, types of mineral present and types of rock clasts were used to provide information on the source rocks responsible for the detrital assemblages. Conglomerate clast composition analysis was performed following the count method of Howard (1993). Prior to data collection, one clast sample from each litho-type was collected from each outcrop and examined under a stereo microscope. Lustre, hardness, shape of grains, phenocrysts and mineral identification were utilized to define the

https://doi.org/10.1017/S0016756823000535 Published online by Cambridge University Press

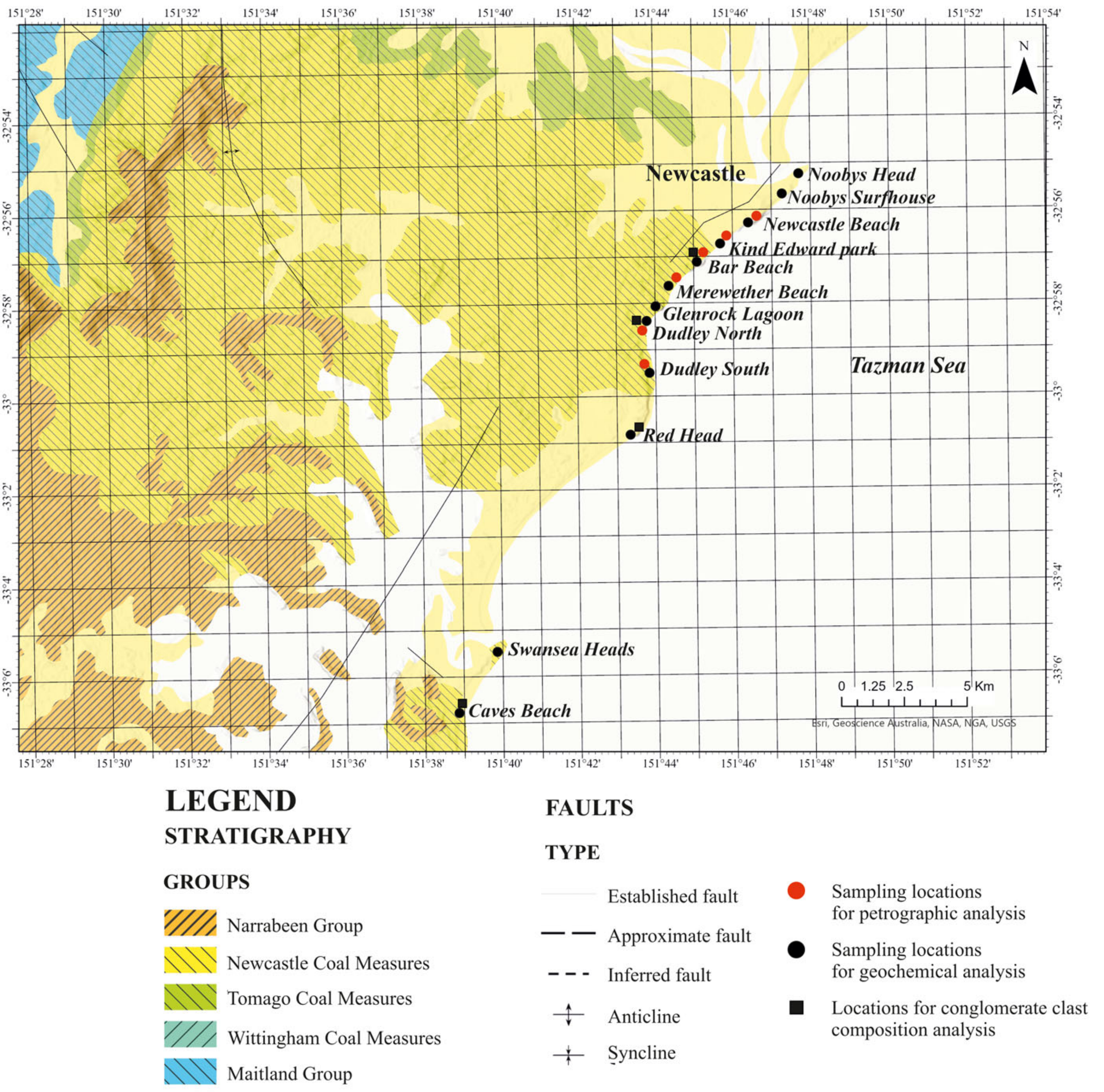

Figure 4. (Colour online) Map of the study region illustrating the lateral extension of the different rock units. Black dots correspond to the selected locations for geochemical analysis, red dots to the locations for petrographic analysis, and black squares to the locations for conglomerate clast composition analysis (modified from Herbert & Helby, 1980).

clast lithology. One hundred clasts were collected at ~10 cm grid intersections in a one square metre area. Three closely spaced subsets (100 clasts each) at each outcrop were obtained and were then integrated for a total of 300 measurements. To maintain high accuracy in the measurements, a minimum cut-off size of 3 mm was established. All clasts less than this threshold were excluded and were considered as matrix since the identification of lithology was uncertain.

Geochemical analysis was carried out by Origin Analytical, using ICP-OES (major elements) and ICP-MS (trace elements and REE), respectively. The geochemical comparison of sedimentary rocks that have accumulated in an inferred tectonic setting with recent, known tectonic settings requires the recalculation to an anhydrous basis of the geochemical data (Rollinson, 1993). In the current study, loss on ignition (LOI) was determined and for statistical coherence, the contents of the major elements in the diagrams were initially recalculated to an anhydrous (LOI-free) basis and then adjusted to 100%. The tectonic setting for the NCM samples was evaluated by using immobile trace elements and the discriminant-function-based multi-dimensional diagrams that utilize major element ratios (the reader is referred to Verma & Armstrong-Altrin, 2013, 2016 for details).

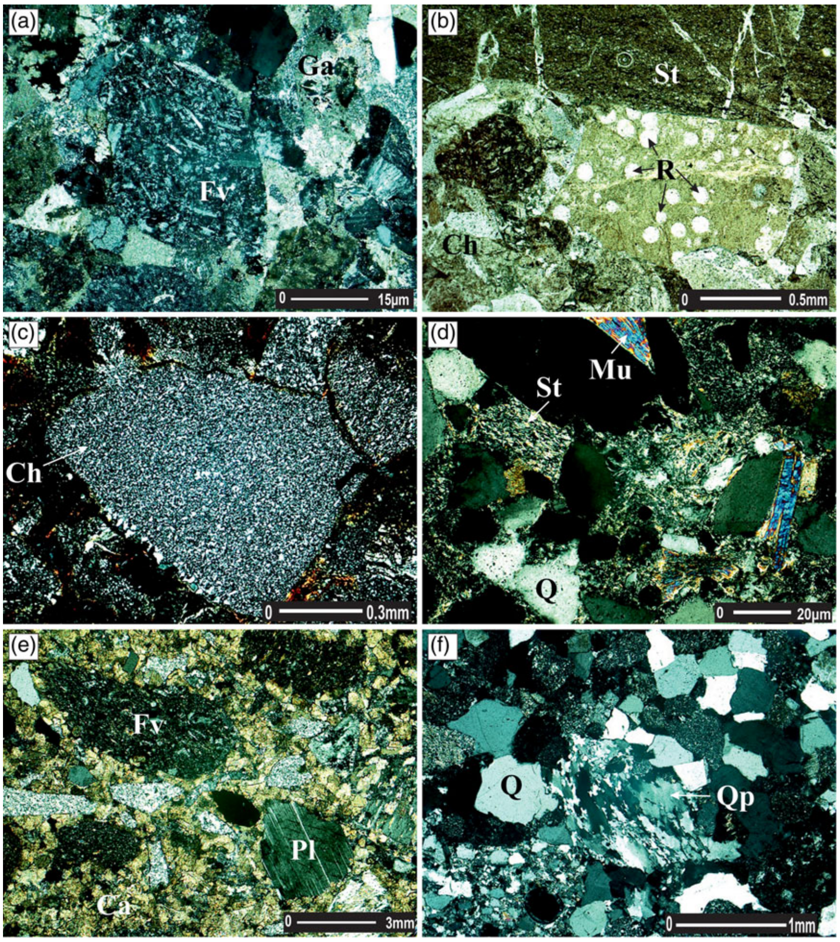

Figure 5. (Colour online) Photomicrographs showing the different types of detritus that occur in the sediments of the NCM. (a) Felsic volcanic clast (Fv) surrounded by secondary calcite aggregates Ca). (b) Possible radiolarians (R) in tuffaceous siltstone host associated with siltstone (St) and chert (Ch) clasts. (c) Chert (Ch) clast showing secondary quartz nucleated at boundary (arrow) XP. (d) Slate (Sl), detrital muscovite (Mu) and quartz (Q). (e) Felsic volcanic clast (Fv) and plagioclase (Pl) surrounded by a calcite cement. Note that many clasts are totally replaced by fine-grained white mica (I. Illite?). (f) Quartz-rich arenite with interlocking, angular to sub-angular quartz (Q) aggregates and polycrystalline quartz (Qp).

4. Results

4.a. Petrography

Sandstone samples from the NCM are poorly to moderately sorted and very fine to coarse-grained. They contain angular to sub-rounded (both mono- and polycrystalline) quartz, plagioclase, K-feldspar and lithic clasts (Fig. 4). Quartz frequently exhibits undulose extinction and/or fractures. Plagioclase is minor, and K-feldspar is uncommon. However, when present, twinning is a common characteristic in K-feldspar minerals. Subhedral to sub-rounded zircon and epidote are accessory minerals. Rare composite grains made up of quartz-plagioclase and graphic intergrowths of quartz-feldspar also occur. Opaque minerals are uncommon. Lithic fragments are abundant and are composed of sedimentary, felsic volcanics (dacitic and rhyodacitic composition) and low-grade metamorphics, such as chert (often radiolarian-bearing), slate, meta-siltstone and quartzite (Fig. 5). Fine-grained mica schist fragments are abundant, while rare granite and hornfels also occur. Some of the clasts are replaced by fine-grained aggregates of white mica (illite?). Pore spaces contain quartz, kaolinite, fine-grained white mica (illite?) and semi-opaque aggregates. The QFL triangular diagram offers information about the composition of the sedimentary rocks, based on the relative abundances of quartz (Q), feldspar (F) and rock fragments (L). The results obtained by the Gazzi-Dickinson point-counting method (Table 1 and S1) were plotted on the QFL triangular diagram (as modified by Garzanti, 2019) to better describe the sandstone composition. The NCM samples plot close to the lines between the transitional arc, the undissected arc and the recycled orogenic fields (Fig. 6a). In the QmFLt triangular diagram (Qm refers to the monocrystalline quartz and Lt to the total amount of lithic clasts), the NCM samples cluster in the lithic recycled field (Fig. 6b). In the QmpFL diagram, the samples plot in the quartzo-lithic field (Fig. 6c). In the LmLvLs triangular diagram (Lm refers to the metamorphic, Lv to volcanic and Ls to sedimentary lithic clasts), the samples plot close to the Lm pole and indicate high contents of metamorphic rock fragments and lesser amounts of sedimentary lithoclasts (Fig. 6d). The NCM samples display no discernible stratigraphic-related petrographic or geochemical trends.

4.b. Conglomerate clast composition

Breckenridge *et al.* (2019) have recently studied the sedimentological aspects of the conglomeratic deposits in the NCM. The conglomerates are clast- to matrix-supported, normally to reversely graded and structureless or cross-stratified. They consist of sub-rounded to well-rounded clasts (granules or pebbles) that occur within a sandy matrix. Clast composition analysis was performed at seven outcrops, and the results indicate that the conglomerates have very similar compositions (Fig. 7). The clasts are composed of (1) igneous rocks clasts of felsic composition, (2) sedimentary rocks clasts, and (3) metamorphic rock clasts. The results from the conglomerate clast composition analysis illustrate the relative proportion of the different rock types. Felsic volcanic rocks and cherts dominate, followed less commonly by mudstone and sandstone.

https://doi.org/10.1017/S0016756823000535 Published online by Cambridge University Press

Table 1. Point-counting data (volume %) for the NCM system

	NCM1 %	NCM2 %	NCM3 %	NCM4 %	NCM5 %	NCM6 %	NCM7 %	NCM8 %	NCM9 %	NCM10 %
Qm	20	16	20	26	28	22	21	21	23	21
Qp	1	2	1	1	1	1	2	1	1	2
Qt	19	15	13	17	14	10	15	12	13	14
C	2	9	9	0	0	0	4	5	5	6
P	4	5	4	4	1	3	2	1	1	2
K	2	3	2	0	0	1	0	0	1	0
Lvh	8	4	4	6	3	7	3	3	2	3
Lm	27	31	34	29	37	35	33	35	34	33
Ls	16	13	13	15	11	19	17	16	16	15
Tqm	0	0	0	0	2	0	1	1	1	0
Mp	0	0	0	0	1	0	1	3	0	1
M	2	3	2	1	1	1	3	2	3	2

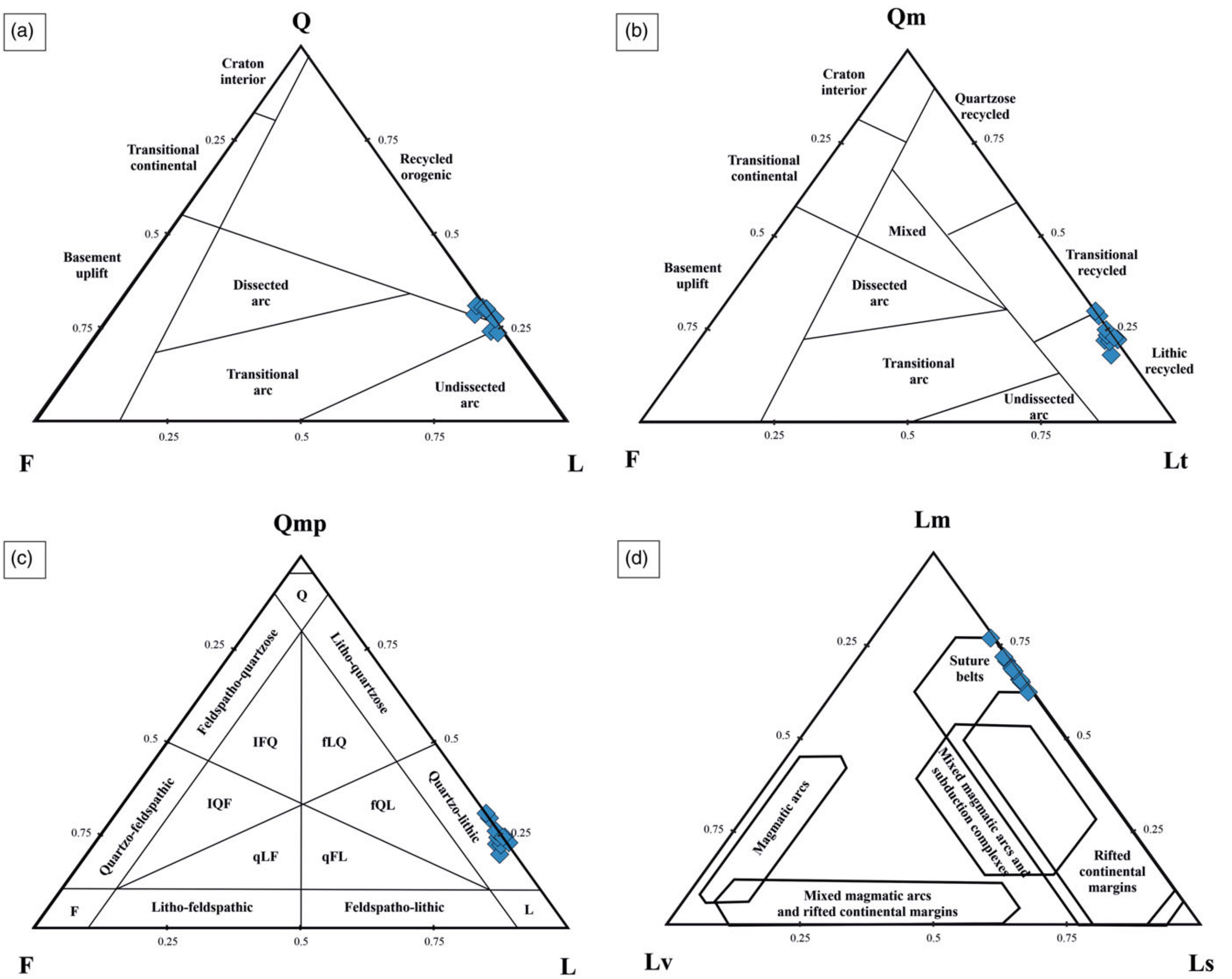

Figure 6. (Colour online) Sandstone composition plots for the NCM samples. (a) QFL compositional plot with Q: quartz; F: feldspar; and L: lithic grains (Dickinson *et al.* 1983). The samples cluster close to the lines between the transitional arc, the undissected arc, and the recycled orogenic fields. (b) QmFLt plot (Dickinson 1985). The samples cluster in the lithic recycled field. (c) QmpFL diagram, where the samples plot in the quartzo-lithic field. (d) Lithic grain diagram that discriminates sedimentary (Ls), volcanic (Lv) and metamorphic (Lm) lithic grains. The samples plot close to the Lm pole.

https://doi.org/10.1017/S0016756823000535 Published online by Cambridge University Press

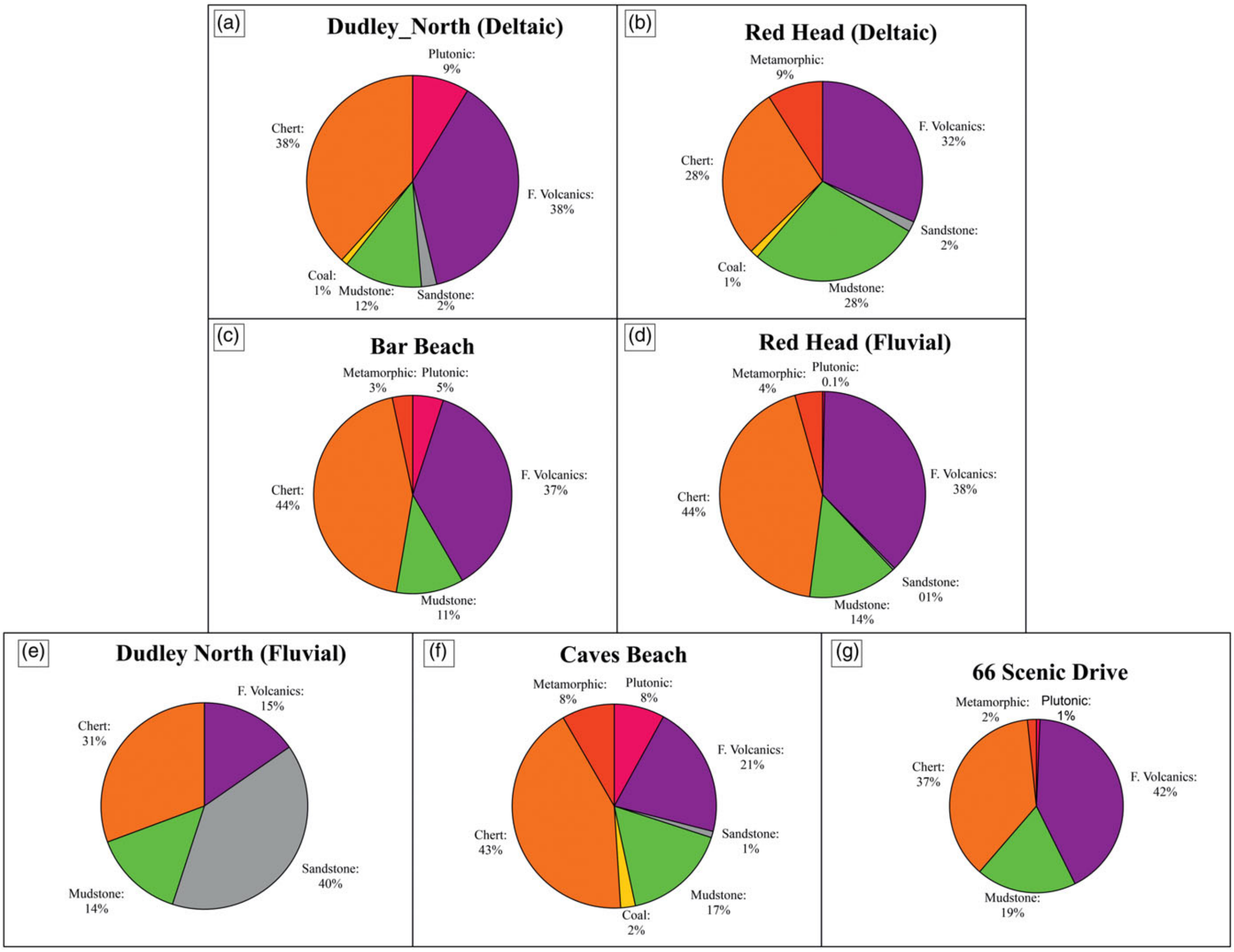

Figure 7. (Colour online) Data from the conglomerate clast composition analysis of the studied NCM sediments. Note the prevalence of a sedimentary source (containing chert, sandstone and mudstone clasts), followed by a felsic volcanic source and a less important metamorphic source.

4.c. Major elements

Most of the major element contents in the NCM samples (Table 2 and S2) are lower than those of the Post-Archean Australian Shale (PAAS). However, SiO_2 (mean 71.2 wt.%) and Na_2O (mean 1.6 wt.%) contents are higher compared to PAAS (62.8 and 1.2 wt.%, respectively, Condie, 1993). The average contents of Al_2O_3 (17 wt%), Fe_2O_3 (3.84 wt%), TiO_2 (0.8 wt%), MgO (1.47 wt%), CaO (0.47 wt%), K_2O (3.35 wt%) and P_2O_5 (0.11 wt%) in the NCM samples indicate that the studied succession is depleted in these major elements relative to the PAAS (18.9, 6.5, 1, 2.2, 1.3, 3.7 and 0.16 wt.%, respectively, Condie, 1993).

Pearson's coefficient correlation variations of major elements (e.g. SiO_2, TiO_2 and K_2O) against Al_2O_3 can reveal the link between the types of minerals and the distribution of major elements (Bauluz *et al.* 2000). The choice of Al_2O_3 is made because Al is little affected by weathering, diagenesis and metamorphism (Bauluz *et al.* 2000). In the samples from the NCM, Al_2O_3 exhibits no significant negative or positive linear correlation with SiO_2, K_2O and TiO_2 (Fig. 8). The K_2O/Al_2O_3 ratios in all samples are below 0.3.

4.d. Trace elements

The trace element abundances of the NCM samples (Table 3 and S2) have been normalized and plotted against Post-Archean Australian Shale (PAAS) for comparison. Average values of Ba, Rb, Sr and Th are 725, 118, 119 and 10 ppm, respectively. Mean U, Zr, Y and Hf concentrations are 2.4, 182, 30 and 5.2 ppm, respectively, and mean Cr, V, Sc, Co, Ni and Cu are 61, 110, 17, 9, 17 and 28 ppm, respectively.

The samples have similar concentrations of the large ion lithophile trace elements (LILE) such as Ba, Rb, Sr, Th and U. Furthermore, they possess similar, but slightly lower abundances of most LILEs relative to PAAS. The NCM samples have similar concentrations of high field strength elements (Zr, Y and Hf) compared to PAAS, but contain lower concentrations of Nb (Fig. 9). The trace elements display no significant correlation with Al_2O_3 (Fig. 8), indicating that weathering associated with clay minerals did not control their abundances and suggesting preservation in primary silicate, oxide and phosphate minerals (Absar & Sreenivas, 2015). The transition trace elements, such as Cr, V, Sc, Co and Ni, have lower concentrations than in PAAS

Table 2. Major elements (in wt.%) after LOI correction for the NCM system

Sample ID	Al_2O_3	SiO_2	TiO_2	Fe_2O_3	MnO	MgO	CaO	Na_2O	K_2O	P_2O_5
1	16.876	73.890	0.906	1.367	0.012	0.858	0.518	0.717	4.825	0.031
2	16.942	71.173	0.861	3.001	0.029	1.419	0.559	2.427	3.514	0.075
3	15.926	71.703	0.862	3.717	0.037	1.695	0.680	1.780	3.465	0.135
4	18.383	72.896	0.925	1.170	0.011	0.945	0.347	1.897	3.167	0.259
5	15.552	65.645	0.795	9.000	0.206	1.835	0.794	1.869	4.138	0.167
6	15.967	71.810	0.737	3.341	0.046	1.352	0.405	2.217	4.008	0.118
7	15.375	69.183	0.851	6.499	0.160	1.923	0.719	2.098	3.018	0.174
8	17.763	70.554	0.819	3.653	0.037	1.963	0.226	1.460	3.450	0.074
9	17.151	71.075	0.845	4.076	0.022	1.430	0.355	1.728	3.223	0.094
10	17.460	69.642	0.850	5.218	0.127	1.646	0.482	1.589	2.824	0.162
11	17.574	72.349	0.760	2.974	0.029	1.303	0.361	1.669	2.881	0.099
12	17.989	67.211	0.899	6.480	0.141	1.966	0.476	1.294	3.408	0.135
13	17.615	71.490	0.839	3.437	0.054	1.554	0.410	1.481	3.004	0.117
14	17.376	72.275	0.764	3.179	0.028	1.495	0.316	1.264	3.196	0.107
15	17.611	76.070	0.760	1.101	0.007	0.702	0.391	0.722	2.617	0.020
16	16.592	72.590	0.866	3.321	0.038	1.435	0.482	1.637	3.002	0.038

	SiO2	Al2O3	K2O	TiO2	Ba	Rb	Sr	Th	U	Zr	Y
SiO2	1.00	0.32	-0.19	-0.13	0.21	-0.18	0.09	0.42	-0.38	0.11	-0.49
Al2O3		1.00	-0.37	0.20	-0.04	-0.07	0.29	0.23	-0.25	0.03	-0.02
K2O			1.00	0.16	0.30	0.84	-0.07	-0.25	0.29	-0.26	0.06
TiO2				1.00	0.47	0.15	0.42	-0.41	0.04	-0.21	0.54
Ba					1.00	0.03	0.52	-0.11	0.19	0.19	0.40
Rb						1.00	-0.28	-0.14	0.14	-0.33	-0.11
Sr							1.00	-0.28	0.08	0.01	0.72
Th								1.00	0.11	0.27	-0.37
U									1.00	0.57	0.46
Zr										1.00	0.01
V											1.00

	SiO2	Al2O3	K2O	TiO2	Hf	Cr	V	Sc	Co	Ni	Cu
SiO2	1.00	0.32	-0.19	-0.13	0.13	0.00	-0.48	-0.56	-0.39	-0.50	-0.77
Al2O3		1.00	-0.37	0.20	0.04	0.18	0.03	-0.12	0.03	-0.10	0.04
K2O			1.00	0.16	-0.23	-0.31	-0.16	-0.02	-0.10	-0.10	-0.17
TiO2				1.00	-0.20	0.16	0.44	0.46	0.31	0.16	0.37
Hf					1.00	0.59	0.10	-0.28	-0.18	-0.06	0.03
Cr						1.00	0.59	0.22	-0.15	0.04	0.31
V							1.00	0.56	0.09	0.20	0.71
Sc								1.00	0.40	0.19	0.54
Co									1.00	0.78	0.46
Ni										1.00	0.58
Cu											1.00

Scale	
-1	negative correlation
-0.7	
-0.5	
-0.3	
0	
0.3	positive correlation
0.5	
0.7	
1	

Figure 8. (Colour online) Pearson's correlations for selected major element (SiO_2, TiO_2 K_2O, Al_2O_3) and trace element (Ba, Rb, Sr, Th, Sc, Cr, V, Ni, Co, Zr, U, Y, Hf and Cu) abundances for the studied NCM samples.

https://doi.org/10.1017/S0016756823000535 Published online by Cambridge University Press

Table 3. Trace elements (in ppm) for the NCM system

Sample ID	Ba	Be	Co	Cr	Cs	Cu	Ga	Hf	Mo	Nb	Ni	Pb
1	1083.179	1.246	1.223	51.622	7.613	13.020	17.293	4.411	2.856	8.948	3.107	11.678
2	1311.862	2.336	6.532	76.449	6.558	26.280	18.920	6.479	1.083	8.363	23.212	17.252
3	1124.016	2.635	11.922	58.444	7.281	31.786	16.841	4.902	1.036	8.126	25.821	14.888
4	1276.130	2.713	21.812	57.076	6.975	27.399	17.453	4.843	1.071	8.936	23.930	20.011
5	832.037	2.254	14.077	56.859	8.894	31.316	17.564	4.891	0.802	7.951	20.967	20.520
6	462.776	1.685	9.000	54.418	5.830	22.063	15.726	5.429	1.265	7.806	17.837	17.031
7	532.708	1.745	10.753	53.256	5.835	32.645	16.369	4.490	1.032	7.435	18.654	14.369
8	354.662	1.868	9.343	48.698	9.473	29.198	18.558	3.420	0.647	6.443	19.028	13.177
9	399.684	1.746	6.325	62.529	8.081	27.069	17.192	4.814	0.874	8.488	15.002	11.803
10	540.058	1.688	9.565	55.176	7.094	33.974	16.771	4.466	0.964	8.024	18.979	12.177
11	740.360	1.854	5.877	63.888	7.319	26.270	17.674	9.297	0.947	9.124	14.598	16.839
12	510.248	2.344	8.797	71.989	10.447	51.580	20.145	5.351	0.953	8.945	16.262	18.492
13	562.008	1.843	13.213	64.882	7.969	33.504	20.034	5.081	1.301	9.199	25.683	14.398
14	526.787	1.917	7.039	59.763	8.815	24.751	19.452	4.234	0.733	8.192	16.597	13.004
15	628.979	1.109	1.732	61.456	3.477	8.110	17.544	4.925	0.545	8.014	1.899	32.371
16	724.842	2.328	7.253	74.854	5.336	31.236	19.432	6.808	0.687	8.153	11.281	15.753

	Rb	Sc	Sn	Sr	Ta	Th	Tl	U	V	W	Y	Zn	Zr
1	161.881	14.642	2.567	85.733	0.731	10.261	0.566	2.455	102.896	3.868	23.576	60.580	140.938
2	110.998	16.851	2.258	119.259	0.713	10.776	0.315	2.625	112.523	1.923	29.370	202.712	233.066
3	116.719	17.584	2.216	110.611	0.682	9.625	0.536	2.390	112.523	3.592	35.995	142.617	167.885
4	102.869	18.511	2.193	377.283	0.715	9.769	0.316	2.401	100.489	1.999	47.723	301.058	164.122
5	135.988	21.075	2.550	122.275	0.690	10.907	0.712	2.861	116.535	2.518	39.067	95.269	166.360
6	120.833	13.909	2.479	108.197	0.657	10.756	0.456	2.727	83.289	2.162	28.270	114.559	192.391
7	97.720	17.996	2.284	105.482	0.627	8.929	0.334	2.255	110.217	3.644	30.711	97.375	158.631
8	136.690	18.248	2.448	82.093	0.621	9.462	0.442	1.877	100.990	2.114	23.146	116.113	111.550
9	114.511	16.886	2.513	96.020	0.709	10.877	0.400	2.499	117.036	1.910	29.340	87.172	172.766
10	109.392	16.828	2.412	106.790	0.664	9.512	0.385	2.286	112.624	2.123	30.071	89.152	154.971
11	108.690	12.650	2.429	110.410	0.778	11.069	0.381	2.729	103.798	2.088	26.538	109.414	344.922
12	130.167	20.549	2.429	86.910	0.762	11.342	0.582	2.809	133.383	2.183	39.267	147.277	186.290
13	112.002	15.535	2.663	103.471	0.758	10.796	0.471	2.558	119.142	2.428	29.541	103.977	174.698
14	124.948	15.203	2.562	109.505	0.731	11.089	0.470	2.373	118.139	2.380	26.799	92.706	136.769
15	99.346	16.565	2.193	61.248	0.651	14.412	0.362	2.036	90.340	2.396	17.752	65.231	170.630
16	114.511	20.331	2.656	130.118	0.729	11.695	0.510	2.791	132.982	2.272	33.043	103.589	242.930

(Fig. 8). The samples have lower abundances of Cu relative to PAAS. The correlation between Al_2O_3 and Co, Cr, Ni and Sc is not statistically significant for the NCM samples (Fig. 8).

4.e. Rare earth elements

In the NCM samples, the total REE contents range from 73.4 to 758.6 ppm (mean 180.6 ppm) and the mean light to heavy REE (LREE/HREE) ratios fluctuate between 6 to 14 (average 7.3, Table 4 and S2). In most of the samples, the La_N/Yb_N and La_N/Sm_N ratios (subscript N refers to chondrite-normalized values) range from 5 to 7.8 (average 6.19) and 2.6 to 6.1 (average 3.2), respectively (Table S2). These characteristics suggest moderate LREE enrichment and fractionated REE patterns. The Gd_N/Yb_N ratios in most of the samples range from 0.6 to 1.52 (average 1.29) and display relatively flat heavy REE (HREE) patterns (Fig. 10). Only one sample (sample 4) exhibits elevated La_N/Yb_N and Gd_N/Yb_N ratios (29.5 and 4.8, respectively) that suggest substantial LREE enrichment and fractionated REE patterns, along with steeper heavy REE patterns (Fig. 10). Further, the sample 4 is enriched in middle REE (MREE, Sm – Ho) and displays a steep MREE/HREE slope. Further, sample 15 illustrates a convex REE pattern, steep MREE/HREE slope and HREE enrichment compared to MREE (Fig. 10). The Eu anomaly of the samples is calculated, by using the following formula: $Eu/Eu^* = (Eu)_N/[(Sm)_N \times (Gd)_N)^{1/2}]$. All samples display Eu depletion that ranges from 0.63 to 0.81 (mean

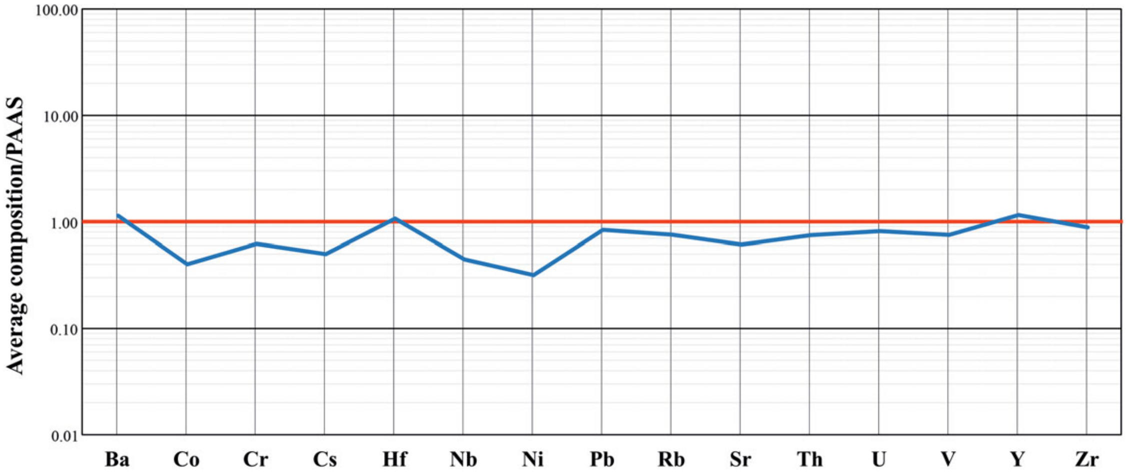

Figure 9. (Colour online) PAAS-normalized multi-element diagram for trace element abundances of the NCM samples (PAAS normalizing values are from Taylor & McLennan, 1985). The trace element values were normalized as ppm. A horizontal line for mudstone PAAS value of 1 is included for reference.

Eu/Eu* = 0.74). The Ce anomaly is calculated using the following formula: $Ce/Ce^* = Ce_N/(Pr_N/La_N)^{1/2}$. All NCM samples exhibit slightly negative Ce anomalies that range from 0.91 to 0.98. N-MORB normalized patterns for the NCM samples show Nb, Ta and Sr depletion and Th enrichment (Fig. 11a), Th/Yb ratios (> 1) and Ta/Yb ratios (> 0.1), indicating that most are geochemically similar (Fig. 11b).

5. Discussion

5.a. Source rock weathering, sorting, and recycling

The data collected in this study indicate that Al_2O_3 does not correlate with any of the oxides. In particular, the absence of a strong negative correlation between Al and Si ($r = 0.09$) suggests that sedimentary sorting and fractionation of framework silicate and phyllosilicate minerals between bedload and suspended load did not take place (Fralick & Kronberg, 1997). One feature that does emerge is that all NCM samples display K_2O/Al_2O_3 ratios below 0.3, indicating that most K_2O occurs in clay minerals ($K_2O/Al_2O_3 < 0.3$, Cox *et al.* 1995), rather than in K-feldspar ($K_2O/Al_2O_3 = 0.3–0.9$). In addition, the lack of correlation between Al_2O_3 and trace elements suggests that that these elements are related to source rocks rather than to clay minerals (Armstrong-Altrin, 2009; Madhavaraju & Lee, 2010). The Index of Compositional Variability (ICV = $(Fe_2O_3 + K_2O + Na_2O + CaO + MgO + MnO + TiO_2)/Al_2O_3$) was utilized to constrain the maturity of the sedimentary source. Sedimentary rocks that are derived from mature source rocks commonly contain a high percentage of clay minerals and exhibit low ICV values (< 1, Cox *et al.* 1995). The samples in this study display mean ICV values (0.7) that are lower than the PAAS (Taylor & McLennan, 1985; ICV = 0.85), suggesting a mature source rock (Table S2). The lack of negative correlation between SiO_2 and Al_2O_3 in the samples (Fig. 12a) suggests a moderate degree of weathering and sorting (Fralick & Kronberg 1997). The degree of weathering has been also estimated based on the correlation of Al_2O_3 with TiO_2 and the Chemical Index of Alteration (CIA = molar $[(Al_2O_3/(Al_2O_3 + CaO^* + Na_2O + K_2O)]) \times 100$; Nesbitt & Young, 1982). In highly weathered rocks, Al_2O_3 displays strong positive correlation with TiO_2, in contrast to sedimentary rocks with a low degree of weathering (Young & Nesbitt, 1999). CIA values increase with increasing degree of weathering (Armstrong-Altrin, 2009). The samples display little correlation between Al_2O_3 and TiO_2, average CIA values of 72.1 similar to PAAS (Taylor & McLennan, 1985; CIA = 70–75) and indicate a moderate degree of weathering.

A moderate degree of weathering is additionally suggested by the Al_2O_3-CaO^* + Na_2O-K_2O (A-CN-K) ternary diagram (Nesbitt & Young, 1984). This diagram illustrates the relationship between Al_2O_3 (aluminous clays), CaO + Na_2O (plagioclase) and K_2O (K-feldspar). Sedimentary rocks that are characterized by increased weathering intensity are concentrated closer to the A axis. The deviation of the weathering trend line from the predicted line, towards the K_2O apex, indicates post-depositional K-metasomatism (Nesbitt & Young, 1984). The NCM samples cluster towards the A axis and along the tonalite-granodiorite predicted weathering trend (Fig. 12b). These characteristics, in conjunction with their distribution, sub-parallel to the A-CN side suggest a moderate degree of source weathering. The degree of sorting and recycling of the samples have been evaluated using the Al_2O_3-Zr-TiO_2 diagram of Garcia *et al.* (1991). In contrast to immature sediments, mature sediments exhibit a wide range of TiO_2/Zr variation (Garcia *et al.* 1991). The samples show no TiO_2/Zr variation and plot close to the PAAS, suggesting a low degree of source sorting and sediment recycling (Fig. 12c). This conclusion is reasonable and compatible with the position of the samples in a fluvio-deltaic system adjacent to the source region (NEO), along with the generally steep topographic gradients (Breckenridge *et al.* 2019). Indeed, the system is coarse-grained and displays an absence of landward penetration of tidal currents into the fluvial realm (from delta-plain to fluvial deposits). These characteristics are common in systems developed under high sediment input, close to the source area.

Summarizing, the sedimentary geochemistry suggests a moderate degree of source weathering and a low degree of source sorting for the NCM samples.

5.b. Provenance

The detritus observed in the sedimentary rocks provides an insight into the sources from which they were derived. Monocrystalline and polycrystalline quartz, fine-grained mica schists, felsic volcanic and low-grade metamorphic clasts are abundant throughout the succession (Fig. 5). Granophyres and granite have also been

Table 4. Rare earth elements (in ppm) for the NCM system

Sample ID	La	Ce	Pr	Nd	Sm	Eu	Gd	Tb	Dy	Ho	Er	Tm	Yb	Lu
1	29.482	57.222	6.712	24.391	4.564	0.939	3.624	0.623	4.038	0.892	2.529	0.404	2.704	0.415
2	30.896	60.718	7.279	27.940	5.414	1.290	4.359	0.761	4.714	1.026	2.920	0.449	3.134	0.458
3	28.029	58.111	7.270	29.183	6.036	1.513	5.825	0.964	5.724	1.201	3.260	0.476	3.138	0.456
4	163.625	336.502	37.779	140.150	25.978	4.866	21.520	2.924	13.478	2.181	4.915	0.587	3.658	0.510
5	32.379	67.320	8.289	33.865	7.147	1.629	6.366	1.088	6.534	1.374	3.763	0.563	3.670	0.549
6	26.457	54.206	6.669	26.787	5.497	1.254	4.842	0.809	4.680	0.989	2.692	0.420	2.809	0.430
7	24.885	51.479	6.418	25.985	5.785	1.315	5.187	0.858	5.153	1.071	3.065	0.438	3.019	0.441
8	24.015	51.499	6.418	24.702	4.788	1.009	3.748	0.642	3.971	0.815	2.404	0.358	2.434	0.372
9	26.773	54.446	6.655	26.125	5.214	1.179	4.483	0.768	4.759	1.044	2.883	0.438	2.786	0.422
10	27.020	55.754	6.951	27.830	5.950	1.392	5.113	0.819	5.102	1.055	2.915	0.445	2.850	0.435
11	30.332	61.577	7.435	29.243	5.658	1.347	4.728	0.762	4.527	0.940	2.562	0.392	2.575	0.370
12	31.489	65.662	7.979	31.890	6.791	1.517	6.197	1.065	6.603	1.400	3.903	0.569	3.832	0.595
13	27.485	55.614	6.775	27.258	5.499	1.314	4.858	0.826	5.052	1.090	2.974	0.455	3.063	0.474
14	27.090	56.783	6.952	26.837	5.277	1.125	4.247	0.737	4.622	0.960	2.725	0.401	2.731	0.410
15	17.668	29.555	3.143	10.707	1.742	0.429	1.623	0.330	2.577	0.653	2.024	0.330	2.314	0.356
16	30.767	60.678	7.287	28.551	5.473	1.256	4.955	0.837	5.446	1.178	3.461	0.517	3.533	0.501

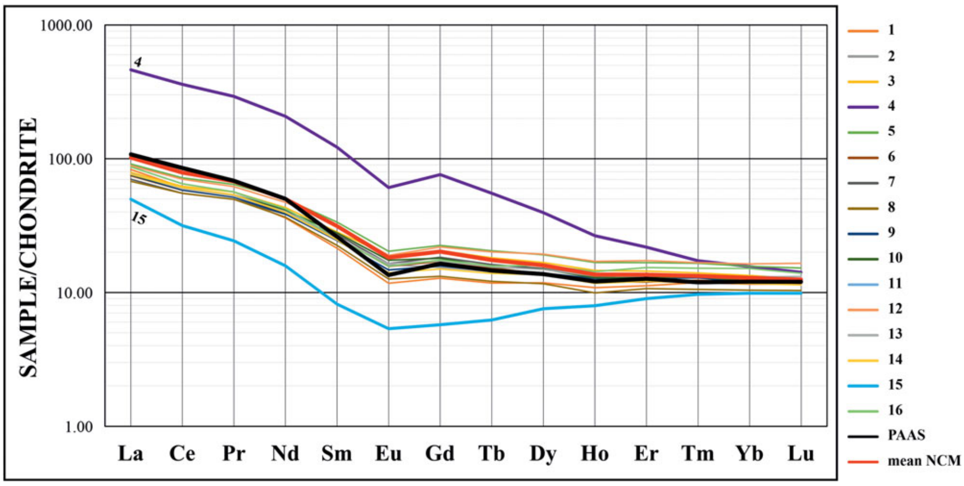

Figure 10. (Colour online) Plot illustrating the chondrite-normalized rare earth element distribution of the NCM samples. Chondrite normalization values are from Taylor and McLennan (1985). REE pattern of Post-Archean Australian Shale (PAAS) is also presented.

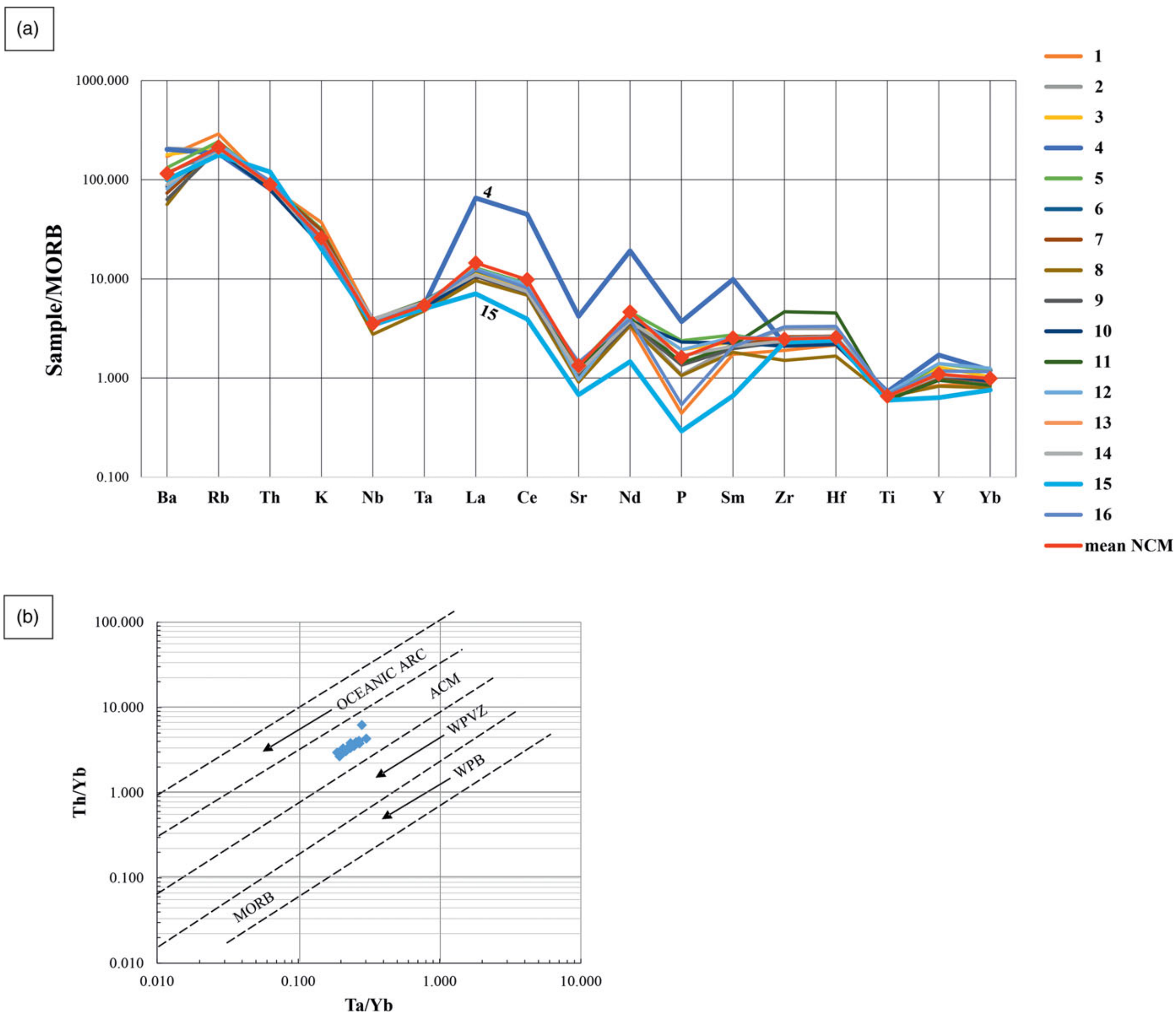

Figure 11. (Colour online) (a). N-MORB normalized patterns of samples from the different depositional environments. The NCM samples exhibit similar features, displaying Nb, Ta depletion, Th enrichment and Sr depletion, suggesting derivation of detritus from calc-alkaline, continental arc rocks (Pearce, 1983). Normalizing values from Sun and McDonough (1989). (b) Th/Yb vs. Ta/Yb plot for intermediate and felsic rocks (Gorton & Schandl 2000). The NCM sample plot in the active continental margin field. Abbreviations: WPB: within-plate basalts, MORB: mid-ocean ridge basalts, ACM: active continental margins, WPVZ: within-plate volcanic zones.

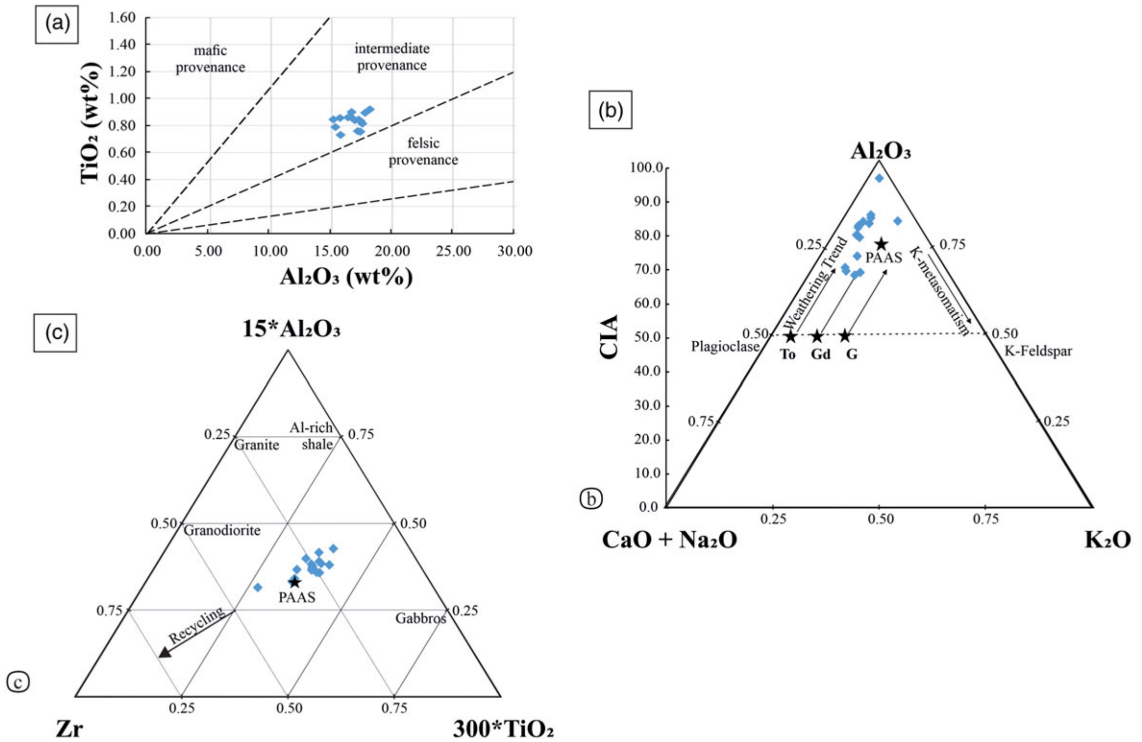

Figure 12. (Colour online) (a) TiO_2 vs. Al_2O_3 plot for the NCM samples (anhydrous-normalized basis) suggesting that all samples have felsic compositions (fields are from Schieber, 1992). (b) A-CN-K diagram (Nesbitt & Young, 1984) that suggests moderate degree of source rock weathering in the NCM. Abbreviations: Ga: gabbro, To: tonalite, Grd: granodiorite, G: granite (Le Maitre, 1976), Pl: plagioclase Ksp: K-feldspar (Nesbitt & Young, 1984), PWT: Predicted weathering trend. (c) $15Al_2O_3$-Zr-$300TiO_2$ ternary diagram (Garcia *et al.* 1991). Arrow points at the typical recycling trend. All plots indicate minimum degree of sediment recycling.

observed in some samples. This indicates that the detritus came from felsic magmatic or volcanic sources. The presence of lithic fragments made up of low-grade metamorphic rocks (meta-siltstone, schist and quartzite), sedimentary rocks (siliceous lutite, chert, mudstone and sandstone) and polycrystalline quartz indicates that additional sources have provided the detritus for the sedimentary rocks. The plot of the NCM samples in the quartzo-lithic field of the QFL diagram supports this conclusion (Fig. 6). This field is associated with detritus that has been derived from low-grade metamorphic rocks (lower-greenschist or blueschist facies) and suggests the unroofing of upper crustal levels (Garzanti, 2019). In addition, this field suggests the contribution of source rocks that are found in subduction/accretion complexes (Garzanti, 2019). Such rocks containing these mineral assemblages are commonly found in the New England Tablelands Complex (Offler, 2005; Phillips *et al.* 2010).

Support for this conclusion comes from the LmLvLs diagram where all the NCM samples plot in the suture zone field (Fig. 6c), suggesting that the source rocks have been derived from convergent settings (e.g. fold and thrust belts and accretionary complexes). The clasts in the conglomerates are of similar composition to those observed in thin sections and confirm the input of felsic volcanic, sedimentary, and low-grade metamorphic sources (Fig. 7). Previous analyses on the composition of the conglomerates that have been conducted in different parts of the SB revealed the same source rock types (Loughnan, 1966; Little, 1994). In these studies, cherts dominate, followed by sandstone, conglomerate and felsic volcanics.

The provenance of the NCM was further evaluated using the chemical composition of the samples. Even though most major elements are not considered as reliable provenance indicators, TiO_2 and Al_2O_3 are utilized to evaluate the source rock composition because Al and Ti are generally immobile during weathering and transportation processes (McLennan *et al.* 1990). The moderate to high Al_2O_3/TiO_2 ratios (18–23, Table S2) and the TiO_2 vs. Al_2O_3 plot suggest that the NCM samples have intermediate compositions (Fig. 12a). The absence of correlation between Al_2O_3 and Co, Cr, Ni and Sc for the NCM samples (Fig. 8) suggests that these elements are associated with source rocks rather than clay minerals (Armstrong-Altrin, 2009). Further, the low concentration of such elements in NCM samples indicates no contribution of mafic and ultramafic source rocks. In addition to Ti and Al, several plots based on immobile trace elements and REEs have been employed to characterize the composition of the source rock (Floyd & Leveridge, 1987; Condie, 1993; McLennan *et al.* 1993). The Th/Sc vs Zr/Sc plot suggests that the samples have been derived from felsic (granodiorite) igneous rocks (Fig. 13a). Similar conclusions can be drawn from the cross-plots of La/Th vs Hf and Co/Th vs. La/Th, which indicate that felsic rocks are the source of detritus in the samples (Fig. 13b and c).

The chondrite-normalized REE patterns and the type of Eu anomaly can also provide insights about the type of source rocks (Armstrong-Altrin, 2009; Absar & Sreenivas, 2015). Felsic igneous rocks display LREE-enriched patterns and exhibit negative Eu anomalies ($Eu/Eu^* < 1$), while mafic igneous rocks are characterized by lower LREE/HREE ratios with little or no negative Eu anomaly (Cullers, 2000). The contribution of felsic source rocks in the NCM is suggested by the characteristics of the chondrite-normalized REE patterns (e.g. LREE enrichment, flat HREE distribution, negative Eu anomaly; Fig. 10). The MREE enrichment of the sample 4 could be ascribed to mixing of water (fresh and seawater) and fractionation by Fe-oxyhydroxides

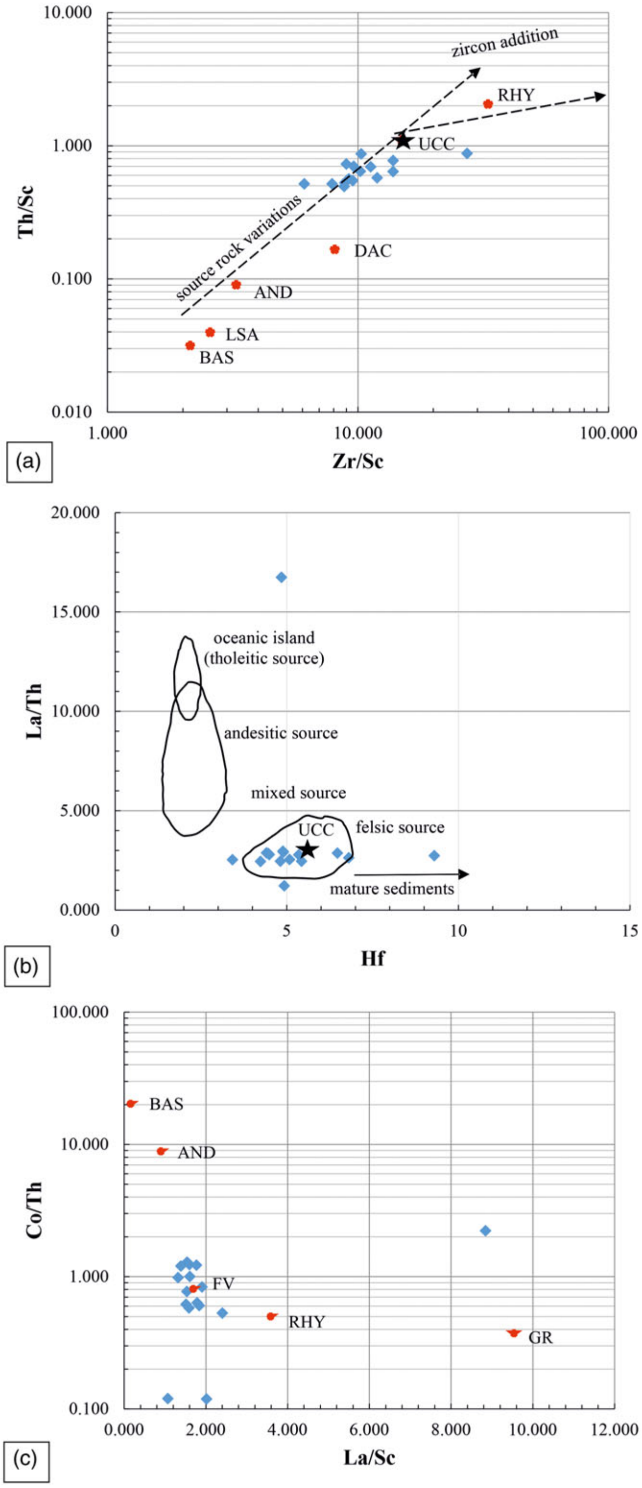

Figure 13. (Colour online) Binary diagrams that evaluate the source rock composition. (a) Th/Sc vs. Zr/Sc diagram. (b) La/Th vs. Hf diagram (Floyd & Leveridge, 1987). (c) Co/Th vs. La/Sc diagram. All three diagrams indicate that the studied deposits were derived from source rocks that are predominantly of felsic composition.

(Bolhar *et al.* 2015). The convex REE patterns and HREE enrichment compared to MREE of sample 15 are probably associated with the presence of phosphates that occupy MREE sites and lead to depletion (Kidder *et al.* 2003; Offler, 2021).

The contribution of detritus to the SB from the rocks in the southern NEO during deposition of sediments in the NCM has been established in several studies (Herbert, 1997; Collins, 2002; Breckenridge *et al.* 2019). The provenance analysis presented here confirms the impact of southern NEO on sedimentation and assigns specific tectonostratigraphic units as source rock candidates. The southern NEO is subdivided into two units, the Tablelands Complex and the Tamworth Belt that are remnants of an older accretion-subduction complex and a forearc basin respectively (Leitch, 1974; Korsch 1977). The data from the petrographic and conglomerate clast composition analyses indicate that chert, sandstone and mudstone were important source rocks for the sedimentary successions in the NCM. Silurian-Devonian chert-rich successions are common in the Tablelands Complex as are Carboniferous turbidites (Djungati and Anaiwan terranes, Aitchison & Flood, 1992) and are thus the most likely source for this rock type (Fig. 1), given that structural and metamorphic data obtained from rocks associated with them suggest a subduction-related origin (Korsch *et al.* 2009a; Phillips *et al.* 2015; Craven & Daczko, 2017). Similar interpretations have been also made from the geochemical analyses (major, trace and REE) on the chert exposures of the Djungati and Anaiwan terranes (Aitchison & Flood, 1992). It is proposed here that the sandstone and mudstone fragments were derived from the Carboniferous turbiditic deposits that occur in the Tablelands Complex (Fig. 1). This conclusion is also supported by the geochemical and petrographic characteristics of these deposits that suggest derivation mainly from felsic sources (dacitic to rhyolitic in composition, Korsch *et al.* 2009a). The LREE enrichment, Nb and Ta depletion and Nb/Yb values>1, shown by all samples (Fig. 11a) is indicative of calc-alkaline, continental arc rocks. This same signature is recorded by sediments in rift basins and accretion-subduction sequences in the Tablelands Complex (Offler, 2021) and points to the Keepit arc being the source.

The fluvio-deltaic system includes thick volcaniclastic deposits (tuffs), suggesting active magmatic activity during the sediment deposition. Geochemical analysis on these tuffs indicates derivation from rhyodacitic to dacitic, continental arc, calc-alkaline magmas and a subduction-related origin (Kramer *et al.* 2001). The Wandsworth Volcanic Group (WVG) crops out from southern Queensland to south of Armidale in the northern margins of the southern NEO (Leitch, 1974). Zircon SHRIMP analysis conducted by Blevin *et al.* (2005) indicates that the WVG spans from 256.4 ± 1.6 Ma (at the base of the WVG) to 254.1 ± 2.2 Ma (Dundee Rhyodacite). These results are identical to the recently obtained high precision CA-TIMS ages of stratigraphically equivalent tuffs in the SB and Bowen Basin (Metcalfe *et al.* 2015; Maravelis *et al.* 2020), indicating that WVG is the principal contributor of volcanic material into these basins. The WVG is composed of calc-alkaline, silicic to intermediate volcanic rocks, with a continental, subduction-related geochemistry (Stewart, 2001). Rocks similar to those in the WVG are not exposed in the study area, but the presence of tuffs indicates contemporaneous volcanic activity. It is possible that such deposits occur offshore and are covered by recent sediments.

To sum up, the most likely sources of the detritus in the NCM are represented by the Tamworth Belt and Tablelands Complex, with the former providing the felsic volcanics, and the latter providing the sandstone, mudstone, slates, polycrystalline quartz and radiolarian-bearing chert/siltstone. Felsic volcanics would also have come from the Tablelands Complex that contains arenites formed from sands derived from the forearc basin adjacent to the Keepit arc that have been subducted.

https://doi.org/10.1017/S0016756823000535 Published online by Cambridge University Press

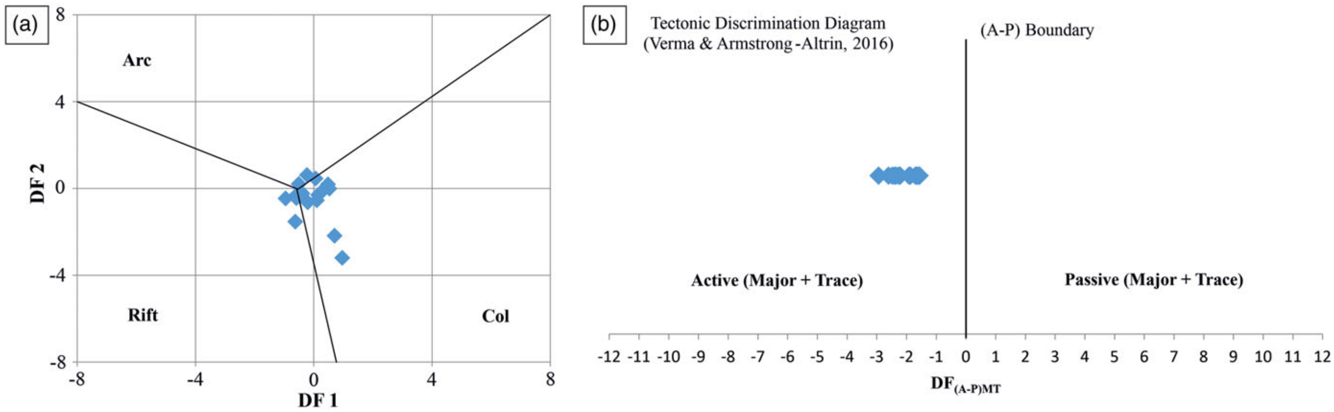

Figure 14. (Colour online) Binary diagrams that evaluate the tectonic setting of the NCM samples. (a) Discriminant function multi-dimensional plot for high-silica clastic sediments (the reader should refer to Verma & Armstrong-Altrin, 2013, for detailed explanation of the discriminant-function equations). The diagram suggests an arc-related tectonic setting under contractional tectonic regime. (b) Major element-based diagram that separates active (A) and passive (P) margins (from Verma & Armstrong-Altrin, 2016). The function (DF (A-P)M) is determined from the equation: DF (A-P)M = (3.0005 × ilr1Ti) + (−2.8243 × ilr2Al) + (−1.0596 × ilr3Fe) + (−0.7056 × ilr4Mn) + (−0.3044 × ilr5Mg) + (0.6277 × ilr6Ca) + (−1.1838 × ilr7Na) + (1.5915 × ilr8K) + (0.1526 × ilr9P) − 5.9948. The diagram suggests an arc-related tectonic setting under contractional tectonic regime.

5.c. Tectonic setting

QFL ternary diagrams can provide information about the tectonic setting of the source rocks, based on the proportion of quartz, feldspar and lithic components (Garzanti, 2019). In this diagram, all NCM samples cluster close to the line between the transitional arc and the recycled orogenic field (QFL, Fig. 6a) and in the lithic recycled field (QmFLt, Fig. 6b). Further, the Th/Yb-Ta/Yb plot of Gorton and Schandl (2000) reveals that the source rocks formed in an active continental setting (Fig. 11b).

To gain further information about the tectonic setting, siliciclastic sediments in the study area have been evaluated using chemically based diagrams (e.g. Bhatia, 1983; Roser & Korsch, 1986; Floyd & Leveridge, 1987; McLennan, 1989; Verma & Armstrong-Altrin, 2013). However, the discrimination diagrams proposed by Bhatia (1983) and Roser and Korsch (1986) have been challenged by several authors (Armstrong-Altrin & Verma, 2005; Ryan & Williams, 2007; Verma & Armstrong-Altrin, 2013; Verma *et al.* 2013) because their proposed tectonic settings are often inconsistent with the regional geology (Valloni & Maynard, 1981; Dostal & Keppie, 2009). The tectonic setting of the different source rocks that contribute to the formation of the sedimentary successions has been determined in recent studies using the diagrams proposed by Verma and Armstrong-Altrin (2013). These diagrams are made for both high (SiO_2 = 63–95%) and low silica (SiO_2 = 35–63%) sediments and group the results into collision, continental or island or arc, and continental rift settings. Even though Neogene to Quaternary sediments were at first employed to test these diagrams, their application expanded to older deposits (Zaid & Gahtani, 2015; Tawfik *et al.* 2017). The results obtained conform to the geological history of the case studies, and thus, these diagrams provide acceptable tectonic settings for the source rocks. This is because they have been constructed, considering the effects of weathering, alteration, recycling, diagenesis and experimental inconsistencies. Further, in contrast to the older methods, the datasets are treated with modern statistical techniques (Verma & Armstrong-Altrin, 2013).

All NCM samples display SiO_2 contents greater than 63%, and therefore, the high-silica diagram was applied for the tectonic discrimination of the source rocks. The samples plot principally on the collision field, with a small number of samples plot on the arc field and one sample on the rift field (Fig. 14a). This diagram suggests that the source rocks come from different geotectonic settings most associated with subduction processes and regional contraction. Further, application of the diagram involving all major elements and some trace elements (Cr, Nb, Ni, V, Y and Z) that has been proposed by Verma and Armstrong-Altrin (2016) illustrates that the NCM samples plot on the passive margin field, which is compatible with sedimentary sources derived from a rift tectonic setting (Fig. 14b).

Petrographic and geochemical analyses are very important in basin analysis; however, they need to be supported by thorough field-based investigations to provide data confirming the tectonic setting of sedimentary basins (Ryan & Williams, 2007; Maravelis *et al.* 2016). Recent sedimentological and sequence stratigraphic studies suggest that the NCM was a volcanically influenced sedimentary basin and was characterized by tectonic uplift and basin confinement (Breckenridge *et al.* 2019). The regional stratigraphy is represented by a fluvio-deltaic system that progrades on relatively steep slopes and under high sediment supply. The sequence stratigraphic analysis suggests sediment deposition during highstand and lowstand systems tracts and thus during relative sea-level rise. The fluvio-deltaic boundary is expressed by a regional-scale erosional surface (the subaerial unconformity) that developed during the falling stage systems tract and relative sea-level fall. These field characteristics are interpreted to be the result of tectonic uplift of the southern NEO (Breckenridge *et al.* 2019). The palaeocurrent directions are towards the southeast to southwest and exhibit a temporal transition from parallel (southeast) to perpendicular (southwest) to the southern NEO (Herbert, 1997; Breckenridge *et al.* 2019). This pattern is compatible with a sedimentary basin that developed at the toe of an evolving orogen. The diagrams proposed by Verma and Armstrong-Altrin (2013, 2016) and presented in this study suggest a depositional setting that received detritus from magmatic and contractional, continental settings for the NCM and agree with the proposed basin-fill conditions. The modal compositions of NCM samples, with elevated contents of metamorphic rock fragments and lesser amounts of sedimentary lithoclasts (Fig. 6d), indicate deposition in the retro side of a foreland basin system. Similar compositions have been reported in Andes, where volcano-plutonic detritus prevails in the pro side of the orogen, whereas quartzo-lithic to quartzose detritus that contains mostly

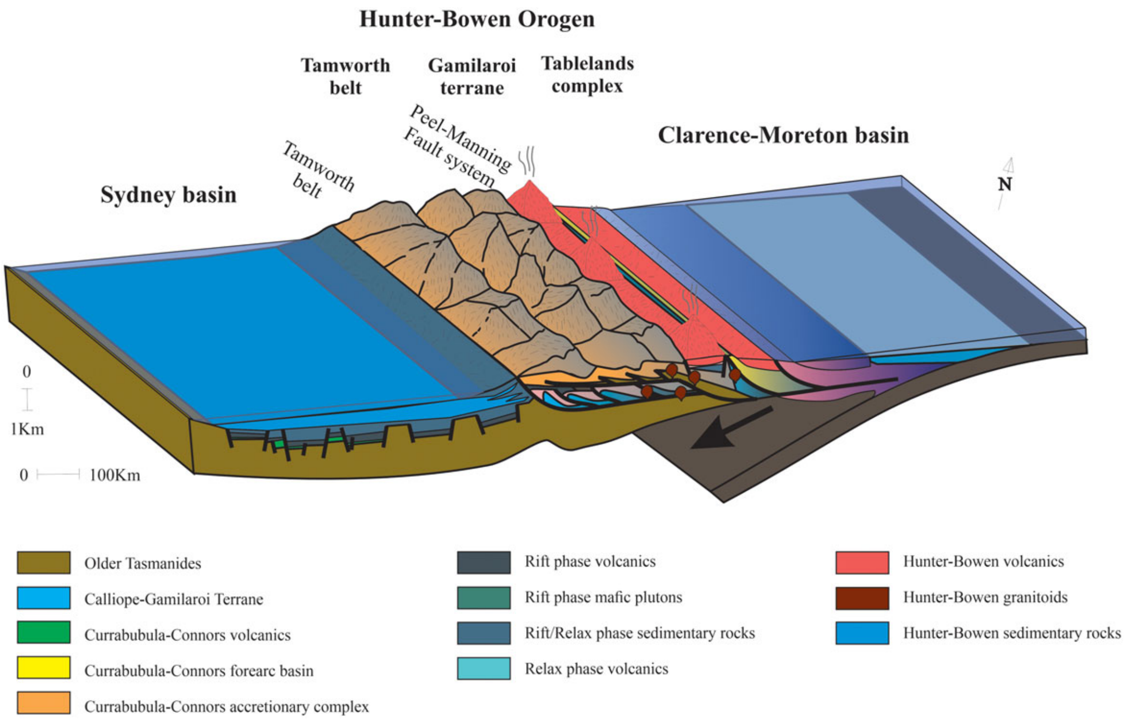

Figure 15. (Colour online) Schematic diagram illustrating the Late Permian geotectonic and depositional setting of the NCM (modified from Jessop *et al.* 2019).

metamorphic lithic grains characterize the retro side (Garzanti *et al.* 2007). The lithic fragments in the NCM samples document prevalence of low-grade metamorphic fragments that could be associated with early syn-collisional stages, when detritus from volcanic arcs and subduction complexes may be abundant. The integration of sequence stratigraphic, palaeocurrent and provenance data confirms that the NCM formed in a retroarc foreland basin, in accordance with earlier studies (Herbert & Helby, 1980; Tye *et al.* 1996; Holcombe *et al.* 1997; Fielding *et al.* 2001; Korsch & Totterdell, 2009).

5.d. Implications for the Late Permian geodynamics of eastern Australia

Eastern Australia was part of the East Gondwanaland from the Cambrian until the Early Cretaceous and part of the convergent plate boundary between the Gondwana and the Proto-Pacific (Panthalassan) Ocean (Collins, 2002; Jenkins *et al.* 2002; Glen, 2005). This plate boundary has experienced recurring periods of contraction and extension, because of trench advance and retreat respectively (Rosenbaum *et al.* 2012; Li & Rosenbaum, 2014; Shaanan *et al.* 2015). In New South Wales (NSW) and along this plate boundary, during the Silurian – Carboniferous time, west-dipping subduction (Offler & Gamble, 2002) occurred, resulting in the development of an accretionary prism (Tablelands Complex) and forearc basin (Tamworth Belt, Korsch, 1977; Korsch *et al.* 2009a). The Tablelands complex is composed of mid-ocean ridge basalt, chert and mudstone that belong to the subducted plate, along with submarine fan deposits and limestone that accumulated in the trench (Aitchison & Flood, 1992). The Silurian to Upper Devonian basalt, chert and mudstone are oceanic in origin and represent the early phases of the accretionary prism, as evidenced by the radiolarian studies (Aitchison *et al.* 1992). The younger submarine fan deposits and limestone (Carboniferous) are the sedimentary products in the trench that have been sourced from the magmatic arc that was active that period (the Currabubula-Connors Arc, Korsch *et al.* 2009b); Craven and Daczko (2017). The Tamworth Belt consists of a wide range of depositional environments, from marginal marine and continental in the western parts, to shallow- and deep-marine in the eastern parts of the forearc basin (Champion, 2016). The sedimentary successions in the Tamworth Belt exhibit a general shallowing-upward trend, from marine environments during the Early Carboniferous, to continental settings during the Late Carboniferous (Roberts *et al.* 2004). The southern NEO lacks volcanic rocks that could be directly associated with the Currabubula-Connors Arc, and its existence is suggested by the occurrence of volcaniclastic material in the Tamworth Belt (Roberts *et al.* 2006). It has been proposed that subsequent contractional tectonics could have buried the magmatic arc under the Tamworth Belt or the younger SB (Korsch *et al.* 1997; Klootwijk, 2013).

During the Late Permian – Mid Triassic time, eastern Australia experienced regional compression because of the westward advance of the subduction zone (Hoy & Rosenbaum, 2017). This stage corresponds to the Hunter-Bowen orogenic event and is responsible for the uplift and development of the southern NEO (Babaahmadi *et al.* 2017) and the transform of the SB into a retroarc foreland basin (Fig. 15). In the southern NEO, this stage leads to accretion of the Silurian – Upper Carboniferous subduction-related provinces (the Tablelands Complex, Tamworth Belt and Currabubula-Connors Arc, Fig. 1). The Hunter-Bowen orogenic event includes three main phases of contraction, a first phase of deformation (~270–260 Ma), a second phase (~253 Ma) and a final phase of deformation (~235–230 Ma, Holcombe *et al.* 1997; Hoy & Rosenbaum, 2017). The first deformational phase was the one responsible for the thickening of the crust and uplift of the Tablelands Complex and Tamworth Belt that constitute the principal components of the southern NEO (Jenkins *et al.* 2002;

https://doi.org/10.1017/S0016756823000535 Published online by Cambridge University Press

Hoy & Rosenbaum, 2017). The Tamworth Belt is accreted on the Tablelands Complex through the Peel-Manning Fault system, whereas the Currabubula-Connors Arc is overthrust by the Tamworth Belt along the Hunter-Mooki Fault (Korsch *et al.* 1997, Fig. 1). The magmatic arc of this stage (the Hunter-Bowen Arc) is positioned east of the Carboniferous Currabubula-Connors Arc (Rosenbaum *et al.* 2012). The Gerringong Volcanics (263–265 Ma; Shi *et al.* 2022) correspond to the oldest products of magmatism and are associated with eastward transportation of volcaniclastic material in the SB (Campbell *et al.* 2001). They indicate the onset of subduction-related magmatism in the evolving NEO and suggest the evolution of the SB as a retroarc foreland basin.

The expansion of the southern NEO and subaerial exposure of Tablelands Complex and Tamworth Belt stimulated excess in sediment supply that was delivered within the adjacent retroarc foreland SB (Diessel, 1992; Jenkins *et al.* 2002; Breckenridge *et al.* 2019, Fig. 15). Thus, the NCM that are the depositional products of this source region uplift should record the provenance and tectonic evolution of the NEO. Indeed, the sequence stratigraphic scenario indicates the progradation (coarsening upward) of the depositional environments and a shoaling upward trend (from delta-front to delta-plain and eventually fluvial setting, Breckenridge *et al.* 2019). These characteristics are likely to be related to the progressively increasing proximity of the NEO to the NCM. Further, the upward shift in palaeocurrent directions (from southeast to southwest) most likely corresponds to the palaeocurrent response of the depositional environments to the Hunter-Bowen orogenic event (Breckenridge *et al.* 2019). During the early stages of NEO uplift, the deltaic drainage systems were characterized by longitudinal flows (parallel to the southern NEO). The later stages include fluvial drainage systems with transverse flows (perpendicular to the southern NEO), reflecting the gradual growth of the NEO and the increase in sediment supply in NCM (Breckenridge *et al.* 2019). The NCM include abundant tuffaceous deposits that document the existence of an active magmatic arc. The age of this magmatism has been elucidated by modern dating techniques (CA-IDTIMS) that revealed an age of ~ 255 Ma (Metcalfe *et al.* 2015; Maravelis *et al.* 2020), indicating the existence of a Late Permian magmatic arc. The upward increase in the abundance of the tuff deposits in NCM (Diessel, 1992) is thought to reflect the approach of the magmatic arc to the NCM and the inboard migration of the arc, towards the edge of the Gondwana continent, during west-directed thrusting associated with the Hunter-Bowen orogenic event (Jenkins *et al.* 2002).

6. Conclusions

The petrographic, geochemical and conglomerate clast composition analysis on the Upper Permian sedimentary succession of the NCM, integrated with sedimentological, palaeocurrent and sequence stratigraphic data, provide insights on the provenance and tectonic setting of the sediments.

Petrographic analysis suggests that sandstone samples from the NCM plot in the quartzo-lithic field contain detritus that has been derived from felsic volcanic and plutonic, low-grade metamorphic and sedimentary rocks. Similar conclusions derive from the conglomerate clast composition analysis that documents the prevalence of tuff, chert, sandstone and mudstone rock fragments. Major element abundances, along with ICV and CIA values, suggest that the NCM samples are geochemically mature and exhibit a moderate degree of source weathering and a low degree of source sorting and sediment recycling. Similar conclusions can be made from the $15Al_2O_3$-Zr-$300TiO_2$ ternary plot. The NCM deposits were derived from felsic source rocks, as suggested by the trace element and REE abundances, in conjunction with the trace element ratios. Discrimination diagrams propose that the source rocks come from an arc-related tectonic setting that experienced regional contraction and agrees with the sequence stratigraphic scenario. It suggests a regional shallowing-upward trend and the development of a sedimentary succession with a regressive architecture that is compatible with the stratigraphic evolution of a retroarc foreland basin. Palaeoflow direction in the deltaic deposits is parallel to the main structural element (southern NEO). However, the palaeoflow direction in the overlying fluvial deposits becomes perpendicular to the structural high, indicating the impact of the evolving orogen on sedimentation.

The integration of provenance, palaeocurrent and sequence stratigraphic analysis indicates that the southern NEO is the principal sediment contributor in the NCM. The Carboniferous arc-forearc basin volcanics and sediments (Tamworth Belt) and Devonian-Carboniferous accretion-subduction complex sequences (Tablelands Complex) most likely offered most of the detritus in the NCM.

Supplementary material. To view supplementary material for this article, please visit https://doi.org/10.1017/S0016756823000535

Acknowledgements. This investigation was sponsored by the New South Wales (NSW) Institute for Frontiers Geoscience (IFG), through the research project: Palaeogeographic and geotectonic evolution of the Myall Trough and Sydney Basin: Constraints in the Palaeozoic geological history of eastern Australia. The authors thank Yanyan Sun (UoN) for preparing the thin sections. The authors would like to acknowledge the two anonymous reviewers for their constructive comments and suggestions that greatly improved the manuscript.

References

Absar N and Sreenivas B (2015) Petrology and geochemistry of greywackes of the ~ 1.6 Ga Middle Aravalli Supergroup, northwest India: evidence for active margin processes. *International Geology Review* **57**, 134–58.

Adekola SA, Akinlua A, Ajayi TR, Adesiyan TA and Ige DO (2018) Geochemistry, heavy mineral and sedimentological analyses of potential reservoir sand samples from Kolmani River-1 well, Northern Benue Trough, Nigeria. *African Journal of Science, Technology, Innovation and Development* **10**, 299–310.

Aitchison JC and Flood PG (1992) Early Permian transform margin development of the southern New England Orogen, eastern Australia (eastern Gondwana). *Tectonics* **11**, 1385–91.

Aitchison JC, Ireland TR, Blake MC and Flood PG (1992) 530 Ma zircon age for ophiolite from the New England Orogen: oldest rocks known from eastern Australia. *Geology* **20**, 125–8.

Armstrong-Altrin JS (2009) Provenance of sands from Cazones, Acapulco, and Bahía Kino beaches, Mexíco. *Revista Mexicana de Ciencias Geológicas* **26**, 764–82.

Armstrong-Altrin JS and Verma SP (2005) Critical evaluation of six tectonic setting discrimination diagrams using geochemical data of Neogene sediments from known tectonic settings. *Sedimentary Geology* **177**, 115–29.

Babaahmadi A, Sliwa R, Esterle J and Rosenbaum G (2017) The development of a Triassic fold-thrust belt in a synclinal depositional system, Bowen Basin (eastern Australia). *Tectonics* **36**, 51–77.

Bauluz B, Mayayo MJ, Fernandez-Nieto C and Gonzalez Lopez JM (2000) Geochemistry of Precambrian and Paleozoic siliciclastic rocks from the Iberian Range (NE Spain): implications for source-area weathering, sorting, provenance, and tectonic setting. *Chemical Geology* **168**, 135–50.

Bhatia MR (1983) Plate tectonics and geochemical composition of sandstones. *Journal of Geology* **91**, 611–27.

Blevin JE, Trigg KR, Partridge ED, Boreham CJ and Lang SC (2005) Tectonostratigraphy and potential source rocks of the Bass Basin: *APPEA Journal* **45**, 601–22.

Bolhar R, Hofmann A, Siahi M, Feng Y and Delvigne C (2015) A trace element and Pb isotopic investigation into the provenance and deposition of stromatolitic carbonates, ironstones and associated shales of the ~3.0 Ga Pongola Supergroup, Kaapvaal Craton. *Geochimica et Cosmochimica Acta* **158**, 57–78.

Bradshaw JD, Vaughan APM, Millar IL, Flowerdew MJ, Trouw RAJ, Fanning CM and Whitehouse MJ (2012) Permo-Carboniferous conglomerates in the Trinity Peninsula Group at Viewpoint, Antarctic Peninsula: sedimentology, geochronology and isotope evidence for provenance and tectonic setting in Gondwana. *Geological Magazine* **149**, 626–44.

Breckenridge J, Maravelis AG, Catuneanu O, Ruming K, Holmes E and Collins WJ (2019) Outcrop analysis and facies model of an Upper Permian tidally influenced fluvio-deltaic system: Northern Sydney Basin, SE Australia. *Geological Magazine* **156**, 1715–41.

Busby CJ, Smith D, Morris W and Fackler-Adams BN (1998) Evolutionary model for convergent margins facing large ocean basins; Mesozoic Baja California, Mexico. *Geology* **26**, 227–30.

Campbell LM, Conaghan PJ and Flood RH (2001) Flow-field and palaeogeographic reconstruction of volcanic activity in the Permian Gerringong Volcanic Complex, southern Sydney Basin, Australia. *Australian Journal of Earth Sciences* **48**, 357–75.

Catuneanu O (2004) Basement control on flexural profiles and the distribution of foreland facies: the Dwyka Group of the Karoo Basin, South Africa. *Geology* **32**, 517–20.

Champion DC (2016) Geodynamic synthesis of the phanerozoic of eastern Australia. Second edition. *Geoscience Australia Record* **07**, 58–82.

Collins WJ (1991) A reassessment of the 'Hunter-Bowen Orogeny': tectonic implications for the southern New England fold belt. *Australian Journal of Earth Sciences* **38**, 409–23.

Collins WJ (2002) Nature of extensional accretionary orogens. *Tectonics* **21**, 1–12.

Condie KC (1993) Geochemical composition and evolution of the upper continental crust: contrasting results from surface samples and shales. *Chemical Geology* **104**, 1–37.

Cox R, Lowe DR and Cullers R (1995) The influence of sediment recycling and basement composition on evolution of mudrock chemistry in the southwestern United States. *Geochimica et Cosmochimica Acta* **59**, 2919–40.

Craven SJ and Daczko NR (2017) The Keepit arc: provenance of sedimentary rocks in the central Tablelands Complex, southern New England Orogen, Australia, as recorded by detrital zircon. *Australian Journal of Earth Sciences* **64**, 401–18.

Cullers RL (2000) The geochemistry of shales, siltstones and sandstones of Pennsylvanian-Permian age, Colorado, USA: implications for provenance and metamorphic studies. *Lithos* **51**, 181–203.

Dickinson WR, Beard LS, Brakenridge GR, Erjavec JL, Ferguson RC, Inman KF, Knepp RA, Lindberg FA and Ryberg PT (1983) Provenance of North American Phanerozoic sandstones in relation to tectonic setting. Geological Society of American *Bulletin* **94**: 222–235.

Dickinson WR (1995) Forearc basins. In *Tectonics of Sedimentary Basins* (eds CJ Busby and RV Ingersoll), pp. 221–61. Blackwell Scientific Publications, Oxford.

Dickinson WR and Suczek C (1979) Plate tectonics and sandstone composition. *American Association of Petroleum Geologists Bulletin* **63**, 2164–82.

Diessel CFK (1992) *Coal-Bearing Depositional Systems*. Berlin: Springer-Verlag, 721 pp.

Dostal J and Keppie JD (2009) Geochemistry of low-grade clastic rocks in the Acatlán Complex of southern Mexico: evidence for local provenance in felsic intermediate igneous rocks. *Sedimentary Geology* **222**, 241–53.

Fielding CR, Sliwa R, Holcombe RJ and Jones AT (2001) A new palaeogeographic synthesis for the Bowen, Gunnedah and Sydney Basins of eastern Australia. In *PESA Eastern Australia Basins Symposium*, Melbourne: The Australasian Institute of Mining and Metallurgy, pp. 269–78.

Floyd PA and Leveridge BE (1987) Tectonic environment of the Devonian Gramscatho basin, south Cornwall: framework mode and geochemical evidence from Turbidite sandstones. *Journal of the Geological Society of London* **144**, 531–42.

Fralick PW and Kronberg BI (1997) Geochemical discrimination of clastic sedimentary rock sources. *Sedimentary Geology* **113**, 111–24.

Garcia D, Coehlo J and Perrin M (1991) Fractionation between TiO_2 and Zr as a measure of sorting within shale and sandstone series (northern Portugal). *European Journal of Mineralogy* **3**, 401–14.

Garzanti E (2019) Petrographic classification of sand and sandstone. *Earth Science Reviews* **192**, 545–63.

Garzanti E, Doglioni C, Vezzoli G and Ando S (2007) Orogenic belts and orogenic sediment provenances. *The Journal of Geology* **115**, 315–34.

Glen RA (2005) The Tasmanides of Eastern Australia: 600 million years of interaction between the proto-Pacific plate and the Australian sector of Gondwana. In A. P. M. Vaughan, P. T. Leat & R. J. Pankhurst (Eds.), Terrane Processes at the Margins of Gondwana. *Geological Society, Special Publication* **246**, 23–96.

Gorton MP and Shandl ES (2000) From continents to island arcs: a geochemical index of tectonic setting for arc-related and within-plate felsic to intermediate volcanic rocks. *Canadian Mineralogist* **38**, 1065–73.

Herbert C (1997) Sequence stratigraphic analysis of early and middle Triassic alluvial and estuarine fades in the Sydney Basin, Australia. *Australian Journal of Earth Sciences* **44**, 125–43.

Herbert C and Helby R (1980) *A Guide to the Sydney Basin*. Sydney: Geological Survey of New South Wales, pp. 1–603.

Hessler AM and Lowe DR (2006) Weathering and sediment generation in the Archean: an integrated study of the evolution of siliciclastic sedimentary rocks of the 3.2 Ga Moodies Group, Barberton Greenstone Belt, South Africa. *Precambrian Research* **151**, 185–210.

Holcombe RJ, Stephens CJ, Fielding CR, Gust D, Little TA, Sliwa R, Kassan J, McPhie J and Ewart A (1997) Tectonic evolution of the northern New England Fold Belt: the Permian-Triassic Hunter-Bowen event, in Tectonics and Metallogenesis of the New England Orogen: Alan H. Voisey Memorial Volume, edited by P. M. Ashley and P. G. Flood. *Geological Society of Australia Special Publications* **19**, 52–65.

Horton BK (2022) Unconformity development in retroarc foreland basins: implications for the geodynamics of Andean-type margins. *Journal of the Geological Society of London* **179**, 263.

Howard JL (1993) The statistics of counting clasts in rudites: a review, with examples from the Upper Palaeogene of southern California, USA. *Sedimentology* **40**, 157–74.

Hoy D and Rosenbaum G (2017) Episodic behavior of Gondwanide deformation in eastern Australia: insights from the Gympie Terrane. *Tectonics* **36**, 1497–520.

Ingersoll RV, Bullard T, Ford R, Grimm J, Pickle J and Sares S (1984) The effect of grain size on detrital modes: a test of the Gazzi Dickinson point counting method. *Journal of Sedimentary Petrology* **54**, 103–16.

Jenkins RB, Landenberger B and Collins WJ (2002) Late Palaeozoic retreating and advancing subduction boundary in the New England Fold Belt, New South Wales. *Australian Journal of Earth Sciences* **49**, 467–89.

Jenkins RB and Offler R (1996) Metamorphism and deformation of an Early Permian extensional basin sequence: the Manning Group, southern New England Orogen. *Australian Journal of Earth Sciences* **43**, 423–36.

Jessop K, Daczko NR and Piazolo S (2019) Tectonic cycles of the New England Orogen, eastern Australia: a review. *Australian Journal of Earth Sciences* **66**, 459–96.

Khazaei E, Mahmoudy-Gharaie MH, Mahboubi A, Moussavi Harami R and Taheri J (2018) Petrography, major and trace elemental geochemistry of the Ordovician-Silurian siliciclastics in north of Tabas Block, Central Iran: implications for provenance and paleogeography. *Journal of Sciences, Islamic Republic of Iran* **29**, 129–42.

Kidder DL, Krishnaswamy R and Mapes RH (2003) Elemental mobility in phosphatic shales during concretion growth and implications for provenance analysis. *Chemical Geology* **198**, 335–53.

Klootwijk C (2013) Middle–Late Paleozoic Australia–Asia convergence and tectonic extrusion of Australia. *Gondwana Research* **24**, 5–54.

Korsch RJ (1977) A framework for the Palaeozoic geology of the southern part of the New England Geosyncline. *Journal of the Geological Society of Australia* **24**, 339–55.

Korsch RJ, Johnstone DW and Wake-Dyster KD (1997) Crustal architecture of the New England Orogen based on deep seismic reflection profiling. In *Tectonics and metallogenesis of the New England Orogen – Alan H. Voisey Memorial Volume* (eds PM Ashley and PG Flood), pp. 29–51. Sydney NSW: Geological Society of Australia, Special Publication 19.

Korsch RJ and Totterdell JM (2009) Subsidence history and basin phases of the Bowen, Gunnedah and Surat Basins, eastern Australia. *Australian Journal of Earth Sciences* **56**, 335–53.

Korsch RJ, Totterdell JM, Cathro DL and Nicoll MG (2009a) Early Permian East Australian Rift system. *Australian Journal of Earth Sciences* **56**, 381–400.

Korsch RJ, Totterdell JM, Fomin T and Nicoll MG (2009b) Contractional structures and deformational events in the Bowen, Gunnedah and Surat Basins, eastern Australia. *Australian Journal of Earth Sciences* **56**, 477–99.

Kramer W, Weatherall G and Offler R (2001) Origin and correlation of tuffs in the Permian Newcastle and Wollombi Coal Measures, NSW, Australia, using chemical fingerprinting. *International Journal of Coal Geology* **47**, 115–35.

Landenberger B, Farrell TR, Offler R, Collins WJ and Whitford DJ (1995) Tectonic implications of Rb-Sr biotite ages for the Hillgrove Plutonic Suite, New England Fold Belt, N.S.W., Australia. *Precambrian Research* **71**, 251–63.

Le Maitre RW (1976) The chemical variability of some common igneous rocks. *Journal of Petrology* **17**, 589–98.

Leitch EC (1974) The geological development of the southern part of the New England fold belt. *Journal of the Geological Society of Australia* **21**, 133–56.

Li P and Rosenbaum G (2014) Does the Manning Orocline exist? New structural evidence from the inner hinge of the Manning Orocline (eastern Australia). *Gondwana Research* **25**, 1599–613.

Li P, Rosenbaum G and Donchak PJT (2012) Structural evolution of the Texas Orocline, eastern Australia. *Gondwana Research* **22**, 279–89.

Little M (1994) Conglomerate composition & palaeocurrent directions in the Newcastle Coal Measures: Implications for non-marine sequence stratigraphy. In *The Twenty Eighth Newcastle Symposium on Advances in the Study of the Sydney Basin* (eds CFK Diessel and RL Boyd), pp. 204–211. Newcastle, NSW Australia: University of Newcastle.

Loughnan FC (1966) A comparative study of the Illawarra Coal measure sediments of the Sydney Basin, New South Wales. *Journal of Sedimentary Petrology* **36**, 1016–25.

Madhavaraju J and Lee YI (2010) Influence of Deccan volcanism in the sedimentary rocks of Late Maastrichtian-Danian age of Cauvery Basin, Southeastern India: constraints from geochemistry. *Current Science* **98**, 528–37.

Maravelis AG, Boutelier D, Catuneanu O, Seymour KST and Zelilidis A (2016) A review of tectonics and sedimentation in a forearc setting: Hellenic Thrace Basin, north Aegean Sea and northern Greece. *Tectonophysics* **674**, 1–19.

Maravelis AG, Breckenridge J, Ruming K, Holmes E, Amelin Y and Collins WJ (2020) Re-assessing the Upper Permian stratigraphic succession of the Northern Sydney Basin, Australia, by CA-IDTIMS. *Geosciences* **10**, 474.

Maravelis AG, Pantopoulos G, Tserolas P and Zelilidis A (2015) Accretionary prism-forearc interactions as reflected in the sedimentary fill of southern Thrace Basin (Lemnos Island, NE Greece). *International Journal of Earth Sciences* **104**, 1039–60.

McLennan SM, Hemming S, McDaniel DK and Hanson GN (1993) Geochemical approaches to sedimentation, provenance and tectonics. In *Processes Controlling the Composition of Clastic Sediments* (eds MJ Johnson and A Basu), Vol. **284**, pp. 21–40. Boulder, CO: Geological Society of America Special Paper.

McLennan SM (1989) Rare earth elements in sedimentary rocks: influence of provenance and sedimentary process. In *Geochemistry and Mineralogy of Rare Earth Elements* (eds BR Lipin and GA McKay), Vol. **21**, pp. 169–200. Washington, DC: Mineralogical Society of America, Reviews in Mineralogy.

McLennan SM, Taylor SR, McCulloch MT and Maynard JB (1990) Geochemical and Nd-Sr isotopic composition of deep-sea turbidites: crustal evolution and plate tectonic associations. *Geochimica et Cosmochimica Acta* **54**, 2015–50.

Melehan S, Botziolis C, Maravelis AG, Catuneanu O, Ruming K, Holmes E and Collins WJ (2021) Sedimentology and stratigraphy of an Upper Permian sedimentary succession: northern Sydney Basin, Southeastern Australia. *Geosciences* **11**, 273.

Menegazzo MC, Catuneanu O and Chang HK (2016) The South American retroarc foreland system: the development of the Bauru Basin in the back-bulge province. *Marine and Petroleum Geology* **73**, 131–56.

Metcalfe I, Crowley JL, Nicoll RS and Schmitz MD (2015) High-precision U-Pb CA-TIMS calibration of Middle Permian to Lower Triassic sequences, mass extinction and extreme climate-change in eastern Australian Gondwana. *Gondwana Research* **28**, 61–81.

Nesbitt H and Young G (1982) Early Proterozoic climates and plate motions inferred from major element chemistry of lutites. *Nature* **299**, 715–17.

Nesbitt HW and Young GM (1984) Prediction of some weathering trends of plutonic and volcanic rocks based on thermodynamic and kinetic considerations. *Geochimica et Cosmochimica Acta* **48**, 1523–34.

Offler R (2005) Metamorphism in the southern New England Fold Belt – an overview. *Geological Society of Australia Abstracts* **76**, 100–4.

Offler R (2021) Geochemistry and provenance of lower Permian sedimentary rocks, Nambucca Block, southern New England Orogen. *Australian Journal of Earth Sciences* **68**, 992–1004.

Offler R and Gamble J (2002) Evolution of an intra-oceanic island arc during the Late Silurian-Late Devonian, New England Fold Belt, Australia. *Australian Journal of Earth Sciences* **49**, 349–66.

Pearce JA (1983) Role of sub-continental lithosphere in magma genesis at active continental margins. In *Continental Basalts and Mantle Xenoliths* (eds CJ Hawkesworth and MJ Norry), pp. 230–249. India: Shiva.

Phillips G, Hand M and Offler R (2010) P–T–X controls on phase stability and composition in LTMP metabasite rocks–a thermodynamic evaluation. *Journal of Metamorphic Geology* **28**, 459–76.

Phillips G, Offler R, Rubatto D and Phillips D (2015) High-pressure metamorphism in the southern New England Orogen: implications for long-lived accretionary orogenesis in eastern Australia. *Tectonics* **34**, 1979–2010.

Roberts J and Engel B (1987) Depositional and tectonic history of the southern New England Orogen. *Australian Journal of Earth Sciences* **34**, 1–20.

Roberts J, Offler R and Fanning M (2004) Upper Carboniferous to Lower Permian volcanic successions of the Carroll–Nandewar region, northern Tamworth Belt, southern New England Orogen, Australia. *Australian Journal of Earth Sciences* **51**, 205–32.

Roberts J, Offler R and Fanning M (2006) Carboniferous to lower permian stratigraphy of the southern Tamworth Belt, southern New England Orogen, Australia: Boundary sequences of the Werrie and Rouchel blocks. *Australian Journal of Earth Sciences* **53**, 249–84.

Rollinson H (1993) *Using geochemical data: Evaluation, presentation, interpretation*. Harlow, UK: Longman, p. 352.

Rosenbaum G, Li P and Rubatto D (2012) The contorted New England Orogen (eastern Australia): new evidence from U-Pb geochronology of early Permian granitoids. *Tectonics* **31**, TC1006.

Roser BP and Korsch RJ (1986) Determination of tectonic setting of sandstone–mudstone suites using SiO_2 content and K_2O/Na_2O ratio. *Journal of Geology* **94**, 635–50.

Rubidge BS, Hancox PJ and Catuneanu O (2000) Sequence analysis of the Ecca-Beaufort contact in the southern Karoo of South Africa. *South African Journal of Geology* **103**, 81–96.

Ryan KM and Williams DM (2007) Testing the reliability of discrimination diagrams for determining the tectonic depositional environment of ancient sedimentary basins. *Chemical Geology* **242**, 103–25.

Schieber J (1992) A combined petrographical-geochemical provenance study of the Newland Formation, Mid-Proterozoic of Montana. *Geological Magazine* **129**, 223–37.

Shaanan U and Rosenbaum G (2018) Detrital zircons as palaeodrainage indicators: insights into southeastern Gondwana from Permian basins in eastern Australia. *Basin Research* **30**, 36–47.

Shaanan U, Rosenbaum G and Wormald R (2015) Provenance of the Early Permian Nambucca block (eastern Australia) and implications for the role of trench retreat in accretionary orogens. *Geological Society of America Bulletin* **127**, 1052–63.

Shi GR, Nutman AP, Lee S, Jones BG and Bann G (2022) Reassessing the chronostratigraphy and tempo of climate change in the Lower-Middle Permian of the southern Sydney Basin, Australia: integrating evidence from U-Pb zircon geochronology and biostratigraphy. *Lithos* **410–411**, 1–21.

Stewart AL (2001) Facies in an Upper Permian volcanic succession, Emmaville Volcanics, Deepwater, northeastern New South Wales. *Australian Journal of Earth Sciences* **48**, 929–42.

Sun S-S and McDonough WF (1989) Chemical and isotopic systematics of oceanic basalts: implications for mantle compositions and processes. In Magmatism in the Ocean Basins (eds AD Saunders and MJ Norry), pp. 313–45. London: Geological Society Special Publication, 42.

Tawfik HA, Salah MK, Maejima W, Armstrong-Altrin JS, Abdel-Hameed AT and Ghandour IM (2017) Petrography and geochemistry of the Lower Miocene Moghra sandstones, Qattara depression, north Western Desert, Egypt. *Geological Journal* **53**, 1938–53.

Taylor SR and McLennan SM (1985) *The Continental Crust: Its Composition and Evolution*. Oxford, UK: Blackwell, pp. 1–349.

Tye SC, Fielding CR and Jones BG (1996) Stratigraphy and sedimentology of the Permian Talaterang and Shoalhaven Groups in the southernmost Sydney Basin, New South Wales. *Australian Journal of Earth Sciences* **43**, 57–69.

Valloni R and Maynard JB (1981) Detrital modes of recent deep-sea sands and their relation to tectonic settings: a first approximation. *Sedimentology* **28**, 75–83.

Veevers JJ (2013) Pangea: Geochronological correlation of successive environmental and strati-tectonic phases in Europe and Australia: *Earth-Science Reviews* **127**, 48–95.

Verma SP and Armstrong-Altrin JS (2013) New multi-dimensional diagrams for tectonic discrimination of siliciclastic sediments and their application to Precambrian basins. *Chemical Geology* **355**, 117–33.

Verma SP and Armstrong-Altrin JS (2016) Geochemical discrimination of siliclastic sediments from active and passive margin settings. *Sedimentary Geology* **332**, 1–12.

Verma SP, Pandarinath K, Verma SK and Agrawal S (2013) Fifteen new-discrimination function-based multidimensional robust diagrams for acid rocks and application to Precambrian rocks. *Lithos* **168**, 113–23.

Weltje GJ (2006) Ternary sandstone composition and provenance: an evaluation of the "Dickinson model". *Geological Society, London, Special Publications* **264**, 79–99.

Young GM and Nesbitt HW (1999) Paleoclimatology and provenance of the glaciogenic Gowganda Formation (Paleoproterozoic), Ontario, Canada: a chemostratigraphic approach. *Geological Society of America Bulletin* **111**, 264–74.

Zaid SM and Gahtani FA (2015) Provenance, diagenesis, tectonic setting and geochemistry of Hawkesbury Sandstone (Middle Triassic), southern Sydney Basin, Australia. *Turkish Journal of Earth Sciences* **24**, 72–98.